

Phase transition and dynamics of water confined in nanoscale spaces

メタデータ	言語: eng 出版者: 公開日: 2017-10-05 キーワード (Ja): キーワード (En): 作成者: メールアドレス: 所属:
URL	http://hdl.handle.net/2297/46579

This work is licensed under a Creative Commons Attribution-NonCommercial-ShareAlike 3.0 International License.



博士論文

Phase transition and dynamics of water
confined in nanoscale spaces

金沢大学大学院自然科学研究科
物質科学専攻

学籍番号 1123132311

氏名 宮東達也

主任指導教員名 水野元博

提出年月 H28年7月

Table of contents

Chapter 1	Introduction.....	1
1.	Water confined with various mesoporous silica.....	1
2.	Water confined with mesoporous silica SBA-16.....	3
3.	Water in sodium chloride aqueous solution confined with mesoporous silica SBA-16.....	4
4.	Hydration water in proteins crystal.....	4
Chapter 2	Experimental detail.....	7
1.	Sample preparations.....	7
2.	NMR measurements.....	8
3.	Differential Scanning Calorimetry (DSC).....	9
Chapter 3	Nuclear Magnetic Resonance (NMR).....	1 2
1.	Simulation of solid-state ^2H NMR spectrum.....	1 2
2.	NMR spin-lattice relaxation time (T_1).....	1 5
3.	NMR spectral density in the case of correlation time distribution.....	1 6
Chapter 4	Water confined with mesoporous silica SBA-16.....	1 7
1.	DSC analysis of phase changes of water confined in SBA-16.....	1 7
2.	NMR spectrum of SBA-16 pore water.....	1 8
3.	Rotational correlation time obtained by ^2H NMR T_1	2 5
4.	Conclusion.....	2 9
Chapter 5	Sodium chloride aqueous solution confined with mesoporous silica SBA-16.....	3 0
1.	Salts concentration inside pore obtained by NMR signal intensity.....	3 0
2.	DSC analysis of sodium chloride aqueous solution confined with SBA-16.....	3 1
3.	^2H NMR spectrum of sodium chloride aqueous solution confined with SBA-16.....	3 3
4.	Rotational correlation time obtained by NMR T_1	3 7
5.	Conclusion.....	4 2
Chapter 6	Hydration water of proteins crystal.....	4 3
1.	^2H NMR spectrum and T_1	4 3
2.	^2H NMR partially relaxed spectrum.....	4 7
3.	Conclusion.....	5 0

Chapter 7 Conclusion	5 1
Reference	5 2
Acknowledgment	5 8
Appendix	5 9

Chapter 1 Introduction

Chapter 1 is introduction of this dissertation entire. This dissertation discusses the physico-chemical property of water confined with nanoscale spaces. In section 1, general property of water confined with various mesoporous silica is described. Additionally, previous research about water confined with various mesoporous silica is presented. Confined water discussed in this dissertation fall into three categories. They are water confined with mesoporous silica SBA-16, water in sodium chloride aqueous solution confined with mesoporous silica SBA-16, and hydration water in the proteins crystal, respectively. The introduction of individual topic is described in greater detail in the following sections. Chapter 2 shows experimental detail containing sample preparation, solid-state NMR measurements and the rest. Chapter 3 shows basic principle of NMR, which is main experimental tool in this dissertation. Measurements and theory used in this dissertation is mainly described. Chapter 4-6 show results, discussions and conclusions of three individual topics. Chapter 7 shows conclusion of this dissertation entire.

1. Water confined with various mesoporous silica

Since the development of well-defined porous silica with programed pore shapes and sizes, there has been marked progress in research on the freezing process of pore water [1, 2, 3, 4, 5, 6, 7, 8, 9, 10] [11, 12, 13, 14, 15, 16]. When free liquid water is statically cooled to below the melting point, 273.2 K, it suddenly freezes at ~ 232 K, and is termed homogeneous nucleation freezing [17]. The spontaneous conversion to ice was observed just below the homogeneous nucleation temperature (HNT) for water microdroplets (~ 10 μm in diameter). In pores, freezing of water is much more complicated in nature, and depends upon pore structure (cylindrical or spherical), size, and connection and, if the pore is connected with external water, the nature of pore surfaces [6, 13, 15]. When water is confined to the cylindrical silica pores ($d < 3.8$ nm), it freezes at temperatures predicted by the Gibbs-Thomson (GT) relation (Equation 1-1), independent of the presence of external water [6, 9].

$$T_0 - T_R = \Delta T = - \frac{2\nu\Delta\gamma_{\text{II-I}}T_0}{\Delta\bar{H}_{\text{II-I}}} \frac{1}{R_{\text{ef}}} \quad \text{Equation 1-1}$$

where T_0 is the melting temperature of bulk ice; T_R is the melting temperature of water frozen in the effective cylindrical pores of radius R_{ef} ($=R-\sigma$: R , pore radius; σ , unfrozen water layer thickness at the solid-liquid interface), and ν is the molar volume of water

which is assumed to be constant during the change in phase. $\Delta \gamma_{II-I}$ and ΔH_{II-I} are the changes in interfacial free energy and enthalpy during the melting of ice (I) to liquid water (II), respectively. Melting temperature is very similar to freezing temperature.

When pore size is larger than 3.8 nm and pore water is not connected to external water, GT relation does not hold. If pore water is not connected to external water, freezing temperature is lower than that predicted by the GT relation but certainly greater than the homogeneous nucleation temperature (HNT) of 232 K; see Figure 1-1.

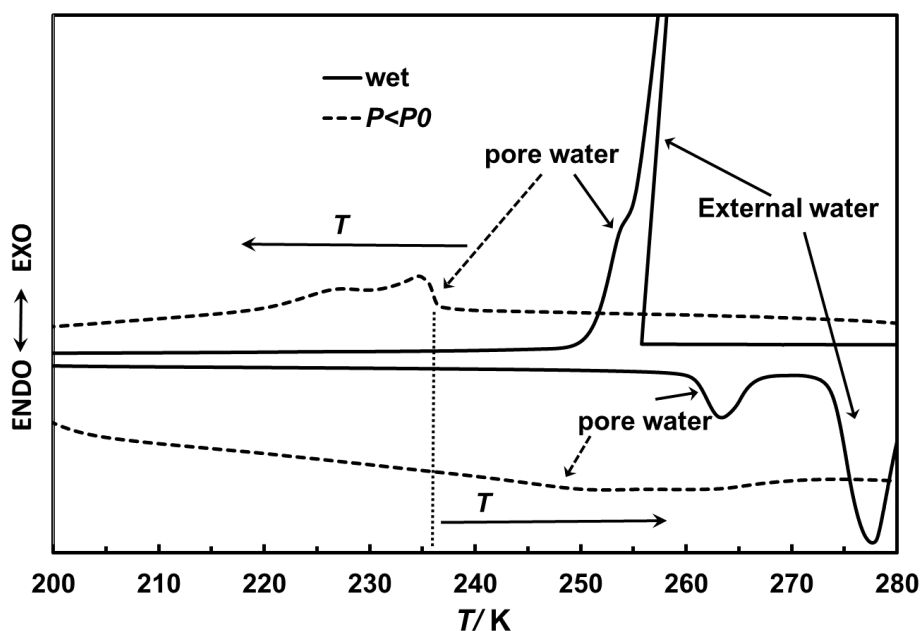


Figure 1-1 DSC curves of D₂O fully and partially confined in MCM-41(C22).

Freezing of pore water in pores smaller than ~ 2.0 nm has not been detected by thermodynamic and structural analyses [9, 11]. Using narrow MCM-41 pores, the low temperature property of unfrozen water has been actively studied, and the transition from high density liquid (HDL) water to low density liquid (LDL) water, which were predicted from the actual phases of high density amorphous ice and low density amorphous ice, was substantiated [7, 11]. However, the liquid-liquid phase transition has been observed only in small cylindrical pores, in which crystal growth is strongly sterically limited. Thus it is suggested that crystallization (crystal growth) of the observed LDL phase is hindered. There are already a number of physico-chemical studies related to this phase transition that used X-ray diffraction, neutron diffractions, NMR, FTIR, thermodynamics, etc [4, 7, 11, 14, 18, 19] [20, 21, 22, 23, 24, 25, 26, 27, 28, 29]. However, those results were explained by the effect of the interfacial property of the pore surface.

Another porous system that has been used to investigate super-cooled liquid water is

cage-like porous silica (e.g. SBA-16 [30, 31], KIT [32] and FDU [33]) in which pore water is frozen constantly at ~ 232 K (HNT) independent of pore size less than $d=8.9$ nm [13]. These spherical pores are large enough for an ice crystallite to grow from the smallest embryo stage of ~ 4.0 nm [10, 34]. Although there have been a number of studies on the utility of chemical reactions as a catalyst [35, 36, 37, 38, 39, 40, 41], it is rare to find detailed studies on the nature of the liquid [42].

2. Water confined with mesoporous silica SBA-16

SBA-16 (SBA=Santa Barbara) is a certain type of mesoporous silica reported by Zhao et. al. [43]. SBA-16 has the three-dimensional pore structure (See Figure 1-2) [44]. SBA-16 has the characteristic spherical mesopores. In addition to the main spherical pores, there are interconnecting channels and micropores, the corona in SBA-16. Thus, the properties of materials involved in this type of porous system must be analysed by accounting for these additional pore components. The pore size of mesopore and the amount of micro pore is controllable by changing the synthesis condition [45, 46, 47]. Before now, there has been many works about SBA-16 containing the application to absorptive medium, catalyst etc. for the good of the controllability of pore shape [48]. With the aim of such application, it is important how the molecules of solute or solvent exist inside mesopores and micropores. In the case of SBA-16, the diffusivity of n-heptane, cumene and mesitylene was confined with the pore was investigated previously [49].

The present study uses solid NMR to study the rotational property of water, D_2O and H_2O included in SBA-16 samples having different pore characteristics. NMR was previously used for cryoporometry on this sample and showed the existence of throat (interconnecting channel) and cage-like pores [50]. However, no detailed study on the nature of pore water exists.

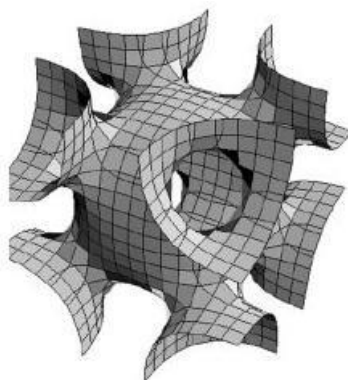


Figure 1-2 The image of mesoporous silica SBA-16 [106].

3. Water in sodium chloride aqueous solution confined with mesoporous silica SBA-16

In the actual application (catalyst, biology, and so on), the system consisting of a single component molecule is rare case. The actual system is almost always more complicated (e.g. multicomponent solution). Then, the property of solution confined with nanoscale spaces is very interesting. The thermodynamics and dynamic property of aqueous solution confined with nanoscale spaces was studied by computer simulation [51, 52, 53, 54, 55], thermal analysis [56, 57], neutron scattering [58], NMR [59] and so on. The vitrification of sodium chloride aqueous solution was induced by the nanoscale confinement [56]. In the case of SBA-16, the proton transport in dilute electrolyte solution confined with SBA-16 was investigated previously [60]. In the case of pure water, water confined with SBA-16 freeze at nearly homogeneous nucleation temperature (HNT) [13]. As adding alkali halide (e.g. sodium chloride) to water, HNT of this bulk aqueous solution decrease until around 195 K with increasing the salt concentration [61]. It is not clear how freezing of aqueous solution confined with nanoscale space is different from that of bulk.

In the present work, the state of sodium chloride aqueous solution confined with SBA-16 was investigated as function of concentration. First, the actual sodium concentration in the pore was determined from the ratio of ^{23}Na NMR signal intensity and ^2H NMR signal intensity. Next, the freezing and melting of aqueous solution in the pore was investigated by DSC and ^2H NMR spectrum. The rotational correlation time of water molecules in the pore was investigated by ^2H NMR T_1 . The correlation time of reconfiguration of water near sodium cation was investigated by ^{23}Na NMR T_1 . The combination of ^2H NMR T_1 and ^{23}Na NMR T_1 can show the dynamics of water molecule as function of distance from sodium cation. The freezing mechanism of aqueous solution and the dynamics of water as changing the salts concentration in the pore of SBA-16 was discussed.

4. Hydration water in proteins crystal

The changes in the structure and dynamics of proteins are caused by glass transition and these changes are directly related to the biological activity of proteins [62, 63, 64, 65].

Figure 1-3 shows the structure of bovine serum albumin (BSA). The glass transition of BSA-water system has been investigated by thermal analysis [66, 67]. A sample quenched from 300 K down to 80 K showed a jump in heat capacity indicating a glass transition temperature T_g of 170 K. When the sample was annealed at 200-240 K, the relaxation effects resulted in three glass transition temperatures: $T_g = 110, 135$ and >180 K. The

glass transition above 180 K is considered to originate from a rearrangement in the motion of the disordered region of the protein. Based on dielectric measurements, the corresponding glass transition was observed at 200 K [68, 69]. The transition accompanying the change in the dynamics of protein and hydration water, also known as the dynamic transition, was found at about 200 K [62, 63, 64, 65]. The glass transitions at $T_g = 110$ and 135 K are considered to be caused by a rearrangement in the motions of primary hydrate water forming a direct hydrogen bond with the protein and part of the internal water localized in the opening of a protein's structure, respectively. Thus, for hydrated proteins, the dynamics of hydration waters plays very important roles in the glass transition. Therefore, detailed analysis of the dynamics of hydration waters around the glass transition is important to investigate the physical properties of proteins. Previously, the relations between the dynamics of hydration waters and the glass or dynamical transition were investigated by various methods [68, 69, 70, 71, 72, 73, 74, 75, 76, 77].

NMR is an effective method to study molecular dynamics and local structures in hydrated proteins [78, 79, 80, 81, 82, 83, 84, 85, 86, 87] [88, 89, 90]. There have been several investigations of the structure and dynamics of BSA using NMR [87, 90]. To investigate the dynamics of water molecules, solid-state ^2H NMR is especially efficient, since the rate and mode of reorientational motions of molecules can be analyzed strictly from the line shape of a broad-line spectrum and T_1 [91, 92, 93, 94, 95, 96, 97, 98, 99, 100] [101]. Thus far, the dynamic properties of hydration waters in elastin, collagen, and myoglobin have been analyzed using ^2H NMR (T_1) [102, 103, 104]. Although the deuteration causes a slight change in its bonding properties, the glass transition behavior and dynamics of water were little affected by deuteration [77]. In the present work, we tried to apply simulation analysis of solid-state ^2H NMR spectra to BSA to obtain more detailed information of the dynamics and structure of hydration waters and to clarify the relations between these two properties and glass transitions. Simulation of ^2H NMR broad-line spectra, including distribution of the motions of water molecules, was performed. Changes in the motional mode, rate and D-O-D angles of hydration waters in BSA with decreasing temperature were investigated using the simulation analysis of ^2H NMR broad-line spectra and T_1 .

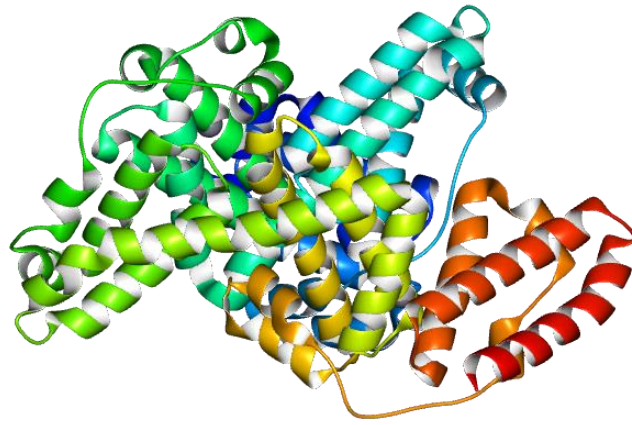


Figure 1-3 The structure of Bovine Serum Albumin(BSA)
[Protein Data Bank Japan (PDBj) PDB ID 3V03]

Chapter 2 Experimental detail

The details of experiments performed in this dissertation is shown in Chapter 2. Section 1 shows the sample preparations for various measurements. Section 2 and Section 3 shows experimental condition of various measurements.

1. Sample preparations

1-1. Water confined with SBA-16

SBA-16 samples were formed as in a previous study [13] (See Figure 2-1). Sample names are as follows: SBA-16(t), where t is the temperature ($^{\circ}\text{C}$) for the preparation of hydrothermal treatments. Pore properties were determined by N_2 adsorption at the temperature of liquid nitrogen and H_2O adsorption at 298.2 K. Pore diameters of pore(cage) are: 6.0 nm for SBA-16(45), 7.0 nm for SBA-16(65), 7.8 nm for SBA-16(80), 8.0 nm for SBA-16(100), and 11.0 nm for SBA-16(120). The pore parameter of SBA-16 prepared in this study is shown in Table 2-1. The samples prepared at ambient conditions were partially hydroxylated with H_2O to form surface OHs. Accordingly, for ^2H NMR measurements, they were thoroughly deuterated as follows. After evacuation by using a turbomolecular pump, samples were exposed to saturated D_2O vapor at room temperature overnight. This process was repeated twice more, followed by suspension in liquid D_2O . This sequential D_2O treatment ensured thorough exchange from the surface of the OH type to that of the OD type. In order to introduce D_2O into the OD type sample, it was suspended in liquid D_2O and internal air in the pores was extracted by evacuation of the suspension to introduce D_2O instead. Samples were precipitated from suspension in the NMR sample holder.

1-2. Sodium chloride aqueous solution confined with SBA-16

The sample used here was SBA-16(80) prepared in previous section. The diameter of pore(cage) was 7.8 nm as previously shown. Prepared SBA-16 powders became mixed with deuterated sodium chloride aqueous solution (0.5 M, 1.0 M, 2.0 M, 4.0M), then the solution was introduced into the pore by expelling any remaining air. The sample for ^2H NMR was sealed in a glass tube 6 mm in diameter and about 25 mm in length. The sample used by ^{23}Na NMR and a part of ^2H NMR was sealed in a polypropylene tube 5 mm in diameter and about 30 mm in length. The excess solution coexisted around SBA-16 powders in a sample tube.

1-3. Hydration water in proteins crystal

Bovine serum albumin(BSA) was obtained from Wako Pure Chemical Industries. BSA powder hydrated with D₂O was prepared by repeated recrystallization three times from D₂O. The hydration level of samples was determined from the observed mass change of dried samples. Although the contents of small particles such as salt ions potentially present may give uncertainty, the hydration level of samples was estimated as $h = 0.26$ (h : gram of water per gram of protein). The sample was sealed in a glass tube 6 mm in diameter and about 20 mm in length.

2. NMR measurements

2-1. ²H NMR

The NMR apparatus used in the case of SBA-16 series and in the case of protein crystals were JEOL ECA 300 and Chemagnetics CMX-300, respectively. The ²H NMR frequencies were 45.282 MHz (JEOL ECA 300) and 45.825 MHz (Chemagnetics CMX-300), respectively. The JEOL NMR probe was used. The sample temperature was controlled with a nitrogen-gas-flow temperature controller (JEOL VT1A). ²H NMR spectrum was conducted by the quadrupole-echo method. The spin-lattice relaxation time T_1 was measured by the inversion recovery method. To avoid the effect of external water or solution, a saturation recovery sequence was employed. The ²H NMR T_1 for frozen ice was sufficiently long, because of slow molecular reorientation [101]. Thus, the NMR signal from frozen ice outside pore was eliminated by the saturation pulse train. The ²H NMR partially relaxed spectrum was observed by a sequence $(90^\circ - \tau_s)_n - \tau_r - 90^\circ_x - \tau_e - 90^\circ_y - \tau_e - \tau_{acq}$ which contain a quadrupole echo method and a saturation recovery method. Here, τ_s , n , τ_r , τ_e , and τ_{acq} are the interval of saturation pulse, the number of saturation pulse, the wait time for spin relaxation, and interval of echo and acquisition time. In the case of SBA-16 series, the 90° pulse width, τ_e , τ_s , and n were 2.8 μ s, 20 μ s, 2 ms and 40, respectively. The wait time τ_r was selected five times as long as T_1 of the fastest relaxation component. In the case of protein crystals, the 90° pulse width, τ_e , τ_s , and n were 2.7 μ s, 20 μ s, 0.1 ms and 5, respectively. Temperature dependence of the NMR signal intensity due to the fraction of spin polarization was corrected under Curie's law. The simulation of ²H NMR spectrum was performed by homemade Fortran programs using double precision [100].

2-2. ¹H NMR

The used apparatus was JEOL ECA 300. The resonance frequency of ¹H NMR was 294.988 MHz. The JEOL static ¹H NMR probe was used. The pulse sequence DEPTH2 was used for background suppression. The 90° pulse width was 1.6 μ s.

2-3. ^{23}Na NMR

The resonance frequency of ^{23}Na NMR was 78.030 MHz. The same NMR probe used at ^2H NMR was used here again. The resonance frequency of the probe was switched by replacing the stick of the condenser. The ^{23}Na NMR spectrum was observed by a single pulse method. ^{23}Na NMR T_1 was measured by the inversion recovery method. To avoid the effect of external solution, a saturation recovery sequence was employed. The ^{23}Na NMR partially relaxed spectrum was observed by a sequence $(90^\circ - \tau_s -)_n - \tau_r - 90^\circ - \tau_{\text{acq}}$ which contain a single pulse method and a saturation recovery method. The 90° pulse width of liquid-state was 1.9 μs . τ_s and n were 2 ms and 40, respectively. The wait time τ_r was selected in a manner completely analogous to ^2H NMR. ^{23}Na NMR Chemical shift were expressed as values relative to 3.0 M deuterated sodium chloride aqueous solution.

2-4. Sodium concentration measurement by using NMR

The standard curve between ^{23}Na NMR signal intensity (I_{Na}) / ^2H NMR signal intensity (I_{D}) and number of sodium cation (N_{Na}) / number of deuterated water molecule ($N_{\text{D}_2\text{O}}$) was made by measuring the deuterated standard sodium chloride aqueous solution ($N_{\text{Na}}/N_{\text{D}_2\text{O}} = 0.073353, 0.03631, 0.01790, \text{ and } 0.009090$). (See Figure 2-2) The deuterated standard sodium chloride aqueous solution was prepared by mixing a certain mass of sodium chloride and heavy water. The sodium chloride (special grade) and heavy water (D, 99.9%) were obtained from Wako Pure Chemical Industries and Cambridge Isotope Laboratories Inc., respectively. The measurements of standard sample were carried out at room temperature. The spectra were observed by a single pulse method. The wait time of the measurement was selected ten times as long as T_1 . The measurements of samples were carried out at room temperature and at 238 K. At 238 K, the sodium chloride aqueous solution outside pore was frozen. The NMR signal of the solution inside pore of SBA-16 was selectively observed by using T_1 and line-shape difference. From the measurements at room temperature, the NMR signal of the solution both inside and outside pore were observed.

3. Differential Scanning Calorimetry (DSC)

DSC measurements were made on samples prepared for the NMR measurements. Wet sediment was placed in an aluminium DSC cell and hermetically sealed. Scanning speed was 5 Kmin^{-1} for both cooling and warming directions. The DSC apparatus used was Q10 (TA Instruments, USA).

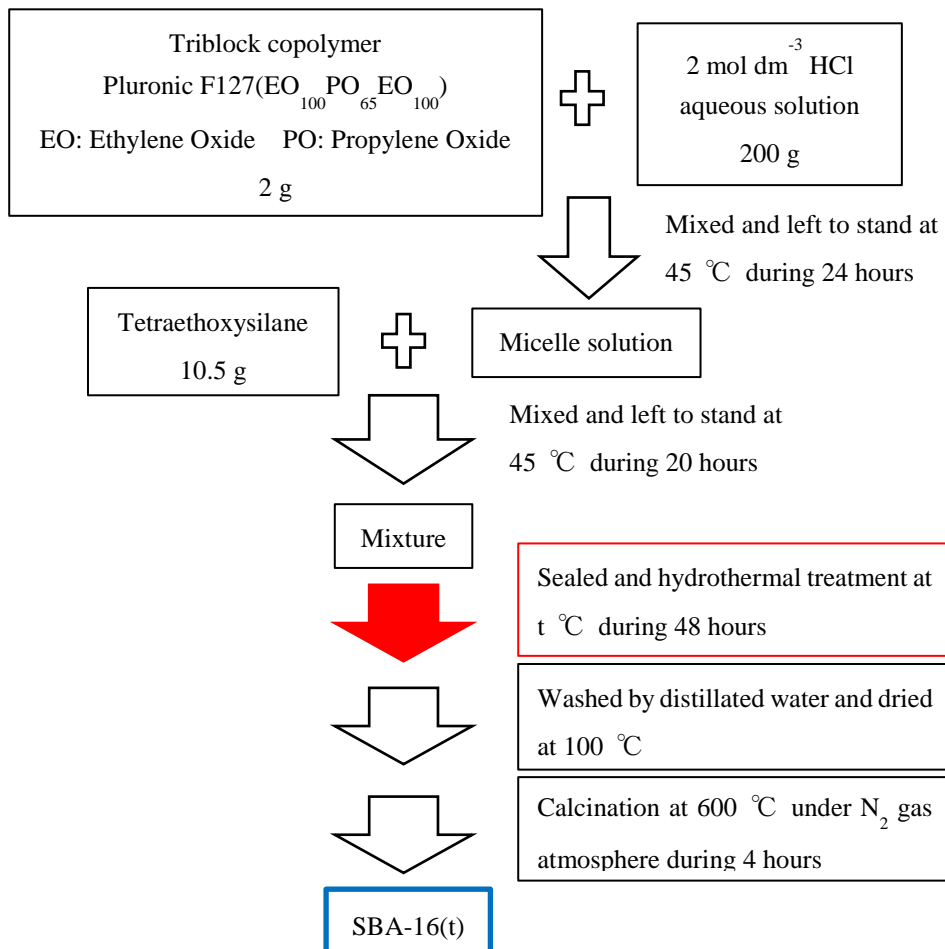


Figure 2-1 Synthetic process of SBA-16 according to ref. [13]. Sample names are as follows: SBA-16(*t*), where *t* is the temperature (°C) for the preparation of hydrothermal treatments.

Table 2-1 The pore parameter of SBA-16 prepared in this study.

	SBA-16(45)	SBA-16(65)	SBA-16(80)	SBA-16(100)	SBA-16(120)
Diameter of spherical mesopore (nm)	4.6	7.0	7.8	8.0	11.0
Ratio of micro pore	0.468	0.462	0.366	0.317	0.053
Diameter of micro pore (nm)	0.72	0.80	0.90	1.0	1.0>

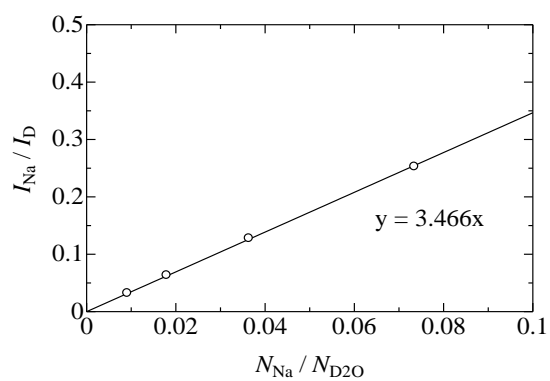


Figure 2-2 Horizontal: Number ratio of sodium cation divided by deuterated water molecule ($N_{\text{Na}}/N_{\text{D}_2\text{O}}$). Vertical: Ratio of ^{23}Na NMR signal intensity divided by ^2H NMR signal intensity ($I_{\text{Na}}/I_{\text{D}}$). The standard curve (solid line) was obtained by measurements of the deuterated standard sodium chloride aqueous solution.

Chapter 3 Nuclear Magnetic Resonance (NMR)

The technical details of NMR measurements mainly used in this dissertation is shown in Chapter 3. Section 1 shows the analysis of ^2H NMR line-shape. Section 2 shows theory of NMR spin-lattice relaxation time (T_1). Section 3 shows handling in the case of distribution of rotational correlation time.

1. Simulation of solid-state ^2H NMR spectrum

^2H nucleus has spin quantum number $I = 1$. In the case of $I \geq 1$, the quadrupolar interaction mainly affects NMR spectrum line-sharp in solid-state. The quadrupolar interaction is the interaction between electric quadrupole moment (eQ) of nucleus and electric field gradient (\hat{V}) at nucleus position. The quadrupolar interaction Hamiltonian is following equation (Equation 3-1).

$$\hat{H}_Q = \frac{eQ}{2I(2I-1)\hbar} \hat{I} \cdot \hat{V} \cdot \hat{I} \quad \text{Equation 3-1}$$

Here, $\hat{I} = (I_x, I_y, I_z)$ is nuclear spin angular momentum operator where z axis is corresponding the direction of static magnetic field in the laboratory (laboratory frame).

In the laboratory frame, \hat{V} is represented by second rank Cartesian tensor (Equation 3-2).

$$\hat{V} = \begin{pmatrix} V_{xx} & V_{xy} & V_{xz} \\ V_{yx} & V_{yy} & V_{yz} \\ V_{zx} & V_{zy} & V_{zz} \end{pmatrix} \quad \text{Equation 3-2}$$

Here, $V_{\alpha\beta} = \frac{\partial}{\partial\alpha} \frac{\partial}{\partial\beta} V$ where V is potential energy of nucleus. \hat{V} matrix can be diagonalized by coordinate rotation to appropriate frame known as principal axis frame.

$$R(\alpha, \beta, \gamma)^{-1} \hat{V} R(\alpha, \beta, \gamma) = \begin{pmatrix} V_{11} & 0 & 0 \\ 0 & V_{22} & 0 \\ 0 & 0 & V_{33} \end{pmatrix} \quad \text{Equation 3-3}$$

Here, $R(\alpha, \beta, \gamma)$ and V_{33}, V_{22}, V_{11} is the rotation matrix of Euler angle (α, β, γ) (Appendix B in ref. [105]) and principle values of tensor, respectively. $V_{33} = eq$, asymmetry parameter

$\eta = \frac{V_{11} - V_{22}}{V_{33}}$ is defined. $\text{Trace}(\hat{V}) = 0$ and the choice of the principal axis ($|V_{33}| \geq |V_{22}| \geq |V_{11}|$)

deduce

$$\hat{V} = R(\alpha, \beta, \gamma) \begin{pmatrix} -\frac{eq}{2}(1-\eta) & 0 & 0 \\ 0 & -\frac{eq}{2}(\eta+1) & 0 \\ 0 & 0 & eq \end{pmatrix} R(\alpha, \beta, \gamma)^{-1} \quad \text{Equation 3-4}$$

The tensor \hat{V} can be represented by eq , η , and (α, β, γ) . The rotation of tensor can be handled by using irreducible spherical tensor more conveniently. The quadrupolar Hamiltonian in the laboratory frame rewritten by using spherical tensor is following equation (Equation 3-5) [105].

$$\hat{H}_Q = \sum_{q=-2}^2 (-1)^q A_{2q}^{LAB} T_{2-q} \quad \text{Equation 3-5}$$

$$T_{20} = \frac{1}{\sqrt{6}} (3I_z^2 - I(I+1)) \quad T_{2\pm 1} = \mp \frac{1}{2} (I_z I_{\pm} + I_{\pm} I_z) \quad T_{2\pm 2} = \frac{1}{2} I_{\pm} I_{\pm}$$

Here, $I_{\pm} = I_x \pm iI_y$ which is known as raising and lowering operator. The irreducible tensor A is transformed under rotation as follow.

$$A_{2q}^{LAB} = \sum_{p=-2}^2 A_{2p}^{PAS} D_{pq}^{(2)}(\psi, \theta, \phi) \quad \text{Equation 3-6}$$

Here, $D_{pq}^{(2)}(\psi, \theta, \phi)$ is second-order Wigner rotation matrix (Appendix B in ref. [105]) of Euler angle (ψ, θ, ϕ) for transformation from the principal axis frame to the laboratory frame. The irreducible tensor A^{PAS} in the principal axis frame is as follow.

$$A_{20}^{PAS} = \frac{3}{\sqrt{6}} \frac{e^2 q Q}{2I(2I-1)\hbar}, A_{2\pm 1}^{PAS} = 0, A_{2\pm 2}^{PAS} = \frac{1}{2} \frac{e^2 q Q}{2I(2I-1)\hbar} \eta$$

As using first-order perturbation theory and in the case of $I=1$, quadrupolar angular frequency is deduced as follow.

$$\omega(\theta, \phi) = \frac{3\pi}{4} \frac{e^2 q Q}{h} [(3\cos^2 \theta - 1) - \eta \sin^2 \theta \cos 2\phi] \quad \text{Equation 3-7}$$

NMR frequency do not depend on ψ because the laboratory is equivalence under axial rotation of the direction of static magnetic field. In the case of powder sample, NMR free induction decay (FID) is calculated as follow.

$$f(t) = \frac{1}{4\pi} \int_0^{2\pi} \int_0^{\pi} \frac{1}{2} [\exp(+i\omega(\theta, \phi)t) + \exp(-i\omega(\theta, \phi)t)] e^{-t/T_2} \sin \theta d\theta d\phi \quad \text{Equation 3-8}$$

Here, the sign + and - represent of two kinds of transition $m_z=0 \leftrightarrow m_z=-1$ and $m_z=+1 \leftrightarrow m_z=0$, respectively. NMR spectrum $I(\omega)$ is obtained by Fourier transformation of $f(t)$.

$$I(\omega) = \text{Re} \int_{-\infty}^{+\infty} f(t)e^{i\omega t} dt \quad \text{Equation 3-9}$$

The ^2H NMR spectrum shows characteristic line-shape. Figure 3-1 shows the example of ^2H NMR simulated spectrum. The quadrupole coupling constant e^2qQ/h interacts width of line-shape and asymmetry parameter η affects figure of line-shape.

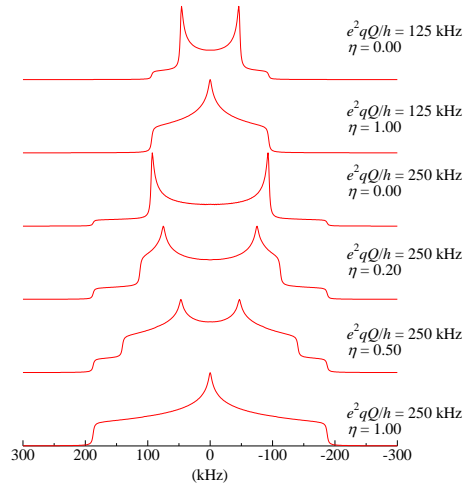


Figure 3-1 Simulated spectrum of solid-state ^2H NMR.

The quadrupolar parameter is shown near the line.

In the case of molecular reorientation, ^2H NMR spectrum is considered. The fast isotropic rotation of molecules eliminates the broadening due to quadrupolar interaction fully. Then, ^2H NMR spectrum become nearly Lorentzian function.

$$I(\omega) = \frac{T_2}{1 + T_2^2 \omega^2} \quad \text{Equation 3-10}$$

Here, T_2 is spin-spin relaxation time. Full Width at Half Maximum (FWHM) of Lorentzian function is related to T_2 as following equation.

$$\text{FWHM} = \frac{1}{\pi T_2} \quad \text{Equation 3-11}$$

So, FWHM is affected by the degree of isotropy of molecular rotation. Other molecular rotation changes the line-shape of ^2H NMR dependent to the geometry of rotation and the rate of rotation. The detail of simulation in the case of molecular reorientation is shown in ref. [100]. Figure 3-2 shows the typical example of ^2H NMR simulated spectrum affected by reorientation of water molecules. ^2H NMR spectrum affected by tetrahedral jump (4 sites jump) is shown in Figure 3-2 (a). This motion is observed in ice I_h crystal [101]. As the jumping rate k increases, the line-shape changes to narrow shape. At fast motion limit, the line-shape of tetrahedral jump is same as isotropic rotation (Lorentzian).

^2H NMR spectrum affected by 180° flip of water (2 sites jump) is shown in Figure 3-2 (b). This motion was often observed in hydration water in metal salt crystals [100, 106] and so on. At fast motion limit, the line-shape of 180° flip is similar to static powder pattern having small e^2qQ/h and large η (See Figure 3-1). In this way, the rate and geometry of molecular motion can be obtained by using simulation analysis of ^2H NMR line-shape.

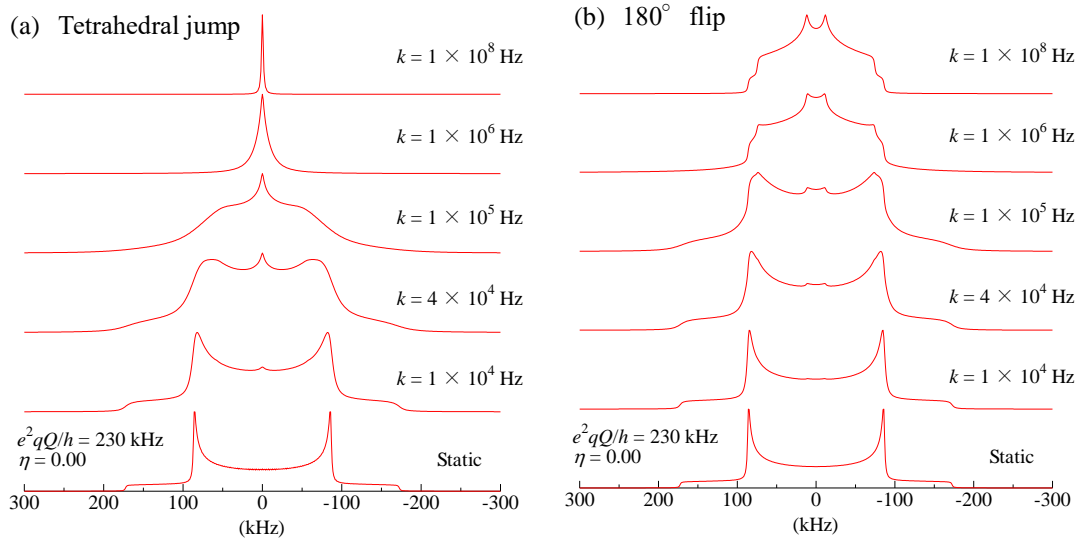


Figure 3-2 Typical example of ^2H NMR simulated spectrum affected by reorientation of water. (a) Tetrahedral jump (e.g. ice) and (b) 180° flip about C_2 axis of water (D-O-D angle = 104 degree).

2. NMR spin-lattice relaxation time (T_1)

In the case of diamagnetic sample, ^2H NMR relaxation is mainly dominated by quadrupolar interaction and molecular rotation. For the isotropic rotation of molecules, $^2\text{H}(I=1)$ NMR T_1 is written as

$$\frac{1}{T_1} = \frac{3\pi^2}{10} \left(\frac{e^2qQ}{h} \right)^2 \left(1 + \frac{\eta^2}{3} \right) \{J(\omega) + 4J(2\omega)\} \quad \text{Equation 3-12}$$

where $J(\omega)$ is spectral density. In the case of single correlation time,

$$J(\omega) = \frac{\tau}{1 + (\omega\tau)^2} \quad \text{Equation 3-13}$$

Here, ω and τ are NMR angular frequency and correlation time of molecular rotation, respectively. For the 180° flip of water molecules, ^2H NMR T_1 is written as

$$T_1^{-1} = \frac{9\pi^2}{40} \left(\frac{e^2qQ}{h} \right)^2 (\sin\theta)^2 \left(\frac{\tau}{1 + (\omega\tau)^2} + \frac{4\tau}{1 + (2\omega\tau)^2} \right) \quad \text{Equation 3-14}$$

where θ is D-O-D angle of water.

In the case of ^{23}Na ($I=3/2$) NMR, longitudinal relaxation with solid-state is biexponential [107]. But, that with liquid-state is exponential due to molecular rotation. Then, the average ^{23}Na NMR T_1 due to isotropic motion is written as

$$\frac{1}{T_1} = \frac{2\pi^2}{25} \left(\frac{e^2 q Q}{h} \right)^2 \left(1 + \frac{\eta^2}{3} \right) \{J(\omega) + 4J(2\omega)\} \quad \text{Equation 3-15}$$

3. NMR spectral density in the case of correlation time distribution

In the case of distribution of rotational correlation time, NMR spectral density $J(\omega)$ is expressed as follow equation.

$$J(\omega) = \int_{-\infty}^{\infty} \frac{\tau}{1 + (\omega\tau)^2} g(\tau/\tau_0) d \ln(\tau/\tau_0) \quad \text{Equation 3-16}$$

Here, $g(\tau/\tau_0)$ is the distribution function of correlation time. In the case of Cole-Cole distribution function (Equation 3-17), the Cole-Cole NMR spectral density $J_{CC}(\omega)$ is written as Equation 3-18 [108].

$$g_{CC}(\tau/\tau_0) = \frac{\sin(\alpha_{CC}\pi)}{2\pi \left[\cosh \left\{ \alpha_{CC} \ln \left(\frac{\tau}{\tau_0} \right) \right\} + \cos(\alpha_{CC}\pi) \right]} \quad \text{Equation 3-17}$$

$$J_{CC}(\omega) = \frac{\sin \left(\frac{\pi}{2} \alpha_{CC} \right) (\omega\tau_{CC})^{\alpha_{CC}}}{\omega \left\{ 1 + (\omega\tau_{CC})^{2\alpha_{CC}} + 2\cos \left(\frac{\pi}{2} \right) (\omega\tau_{CC})^{\alpha_{CC}} \right\}} \quad \text{Equation 3-18}$$

Here, τ_{cc} and α_{cc} indicate the correlation time at the maximum position and the distribution width of correlation time, respectively. $\alpha_{cc}=1$ yields the case of a single correlation time and α_{cc} decreases as the distribution width of correlation time increases. Cole-Cole distribution function is often used as distribution of relaxation time in dielectric relaxation measurement. Cole-Cole distribution has advantages of easy-to-use analysis and comparison to dielectric relaxation measurement.

Chapter 4 Water confined with mesoporous silica SBA-16

Thermodynamic and dynamic properties of water confined in mesoporous silica glass SBA-16 were investigated by DSC, ^1H NMR spectrum and ^2H NMR spin-lattice relaxation time (T_1) as a function of pore size. SBA-16 possesses the main spherical pores, interconnecting channels and micropores (corona). Water in the characteristic spherical pores of SBA-16 freezes at the homogeneous nucleation temperature of water. Between room and freezing temperature, the correlation time of the isotropic rotation of water in the pores of SBA-16 followed the Vogel-Fulcher-Tammann (VFT) relation, which reflects the formation and growth of clusters of fragile water for changing to the strong water. The vitrification of water in micropores around 200 K was observed by ^2H NMR. Above 200 K, the correlation time of the rotation of water in micropores exhibited non-Arrhenius behavior, which is correlated with the gradual decrease in the mobility of water due to the growth of hydrogen bonding, forming low density water before vitrification. After vitrification, the activation energy of the rotation of water in micropores was 25~33 kJmol^{-1} , which was similar to that in ice I_h for all samples. The freedom of cluster formation and water rotation increased with increasing pore size.

1. DSC analysis of phase changes of water confined in SBA-16

Figure 4-1 shows the DSC curves of D_2O confined in SBA-16(45) through SBA-16(120). On cooling, the first exothermic peak appeared at around 262 K in all the samples, but varied from sample to sample. This is ascribed to the freezing of external liquid D_2O . In samples SBA-16(45) through SBA-16(100), a second exothermic peak appeared at 235 K almost independently of the sample or pore size. This is due to the freezing of pore water [13]. In SBA-16(110) and SBA-16(120), freezing of pore water occurred continuously after freezing of external water showing large peaks at 245 K and 240 K, respectively. These peaks can be ascribed to the freezing of water in the pores interconnecting the spherical pores. Small but clear exothermic peaks were seen at 235 K as found in SBA-16(45) through SBA-16(100). Frozen pore D_2O melts at fairly higher temperatures than freezing temperature, and the melting temperature increases as pore size increases; i.e., according to the effect of interfacial energy at the spherical pore surface as suggested by the GT relation. Finally, external D_2O ice melts at 277 K, which is the melting point of D_2O ice. A deconvolution study of peaks using the Gaussian function was conducted but no reasonable explanation could be extracted. However, it is reasonable to assume from the occurrence of a single Gaussian peak that freezing is due to one kind of homogeneous nucleation crystallization of water in the spherical pores.

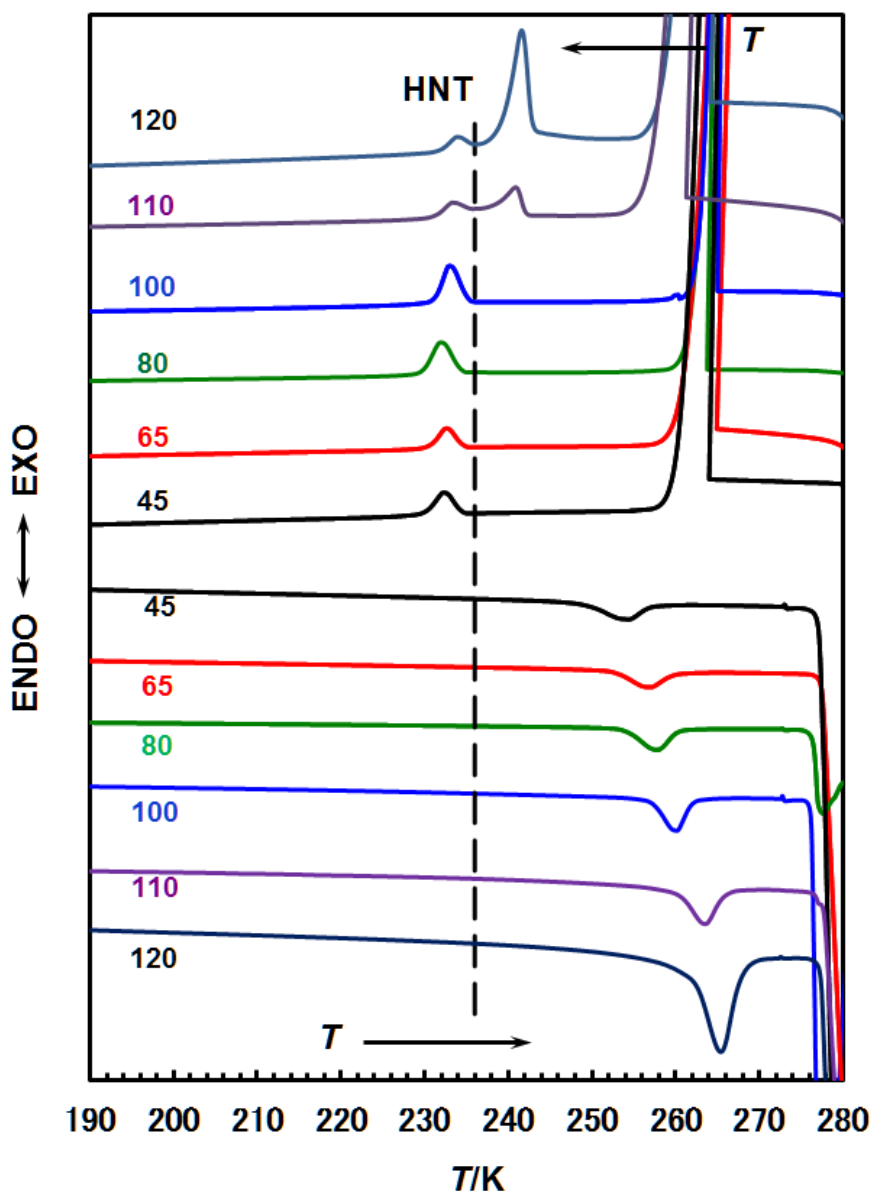


Figure 4-1 DSC curves of D₂O fully confined in SBA-16(45) through SBA-16(120). Numbers near the curves show the temperatures (°C) at which the samples were prepared hydrothermally. Scanning speed for increasing and decreasing temperature is 5 Kmin⁻¹. HNT is the homogeneous nucleation temperature of D₂O ice estimated here.

2. NMR spectrum of SBA-16 pore water

In Figure 4-2 (a) and (b), the ²H NMR spectra of D₂O confined in SBA-16(80) and SBA-16(120) are shown as a function of decreasing and increasing temperatures between 253 and 173 K; the spectra for other SBA-16 samples are given in Figure 4-3 (a)-(c). When temperature decreased, a sharp peak observed at 253 K incorporated an additional wide component, which is characteristic of the quadrupole interaction in the solid phase

because the nuclear spin of deuterium is 1. This peak grew as temperature decreased and the intensity of the sharp peak decreased. This marked change corresponds with the freezing of liquid D₂O confined in the spherical pores of SBA-16, as shown by DSC analysis (Figure 4-1). Heating the samples after cooling down to 173 K caused a reduction in the wide component of ²H NMR spectrum, which remained until 233 K but disappeared at 253 K, instead causing a sharp peak to grow. This change corresponds to the melting of frozen pore D₂O. In fact, the change in peak intensity with temperature varied as the hydrothermal treatment temperature of the sample changed.

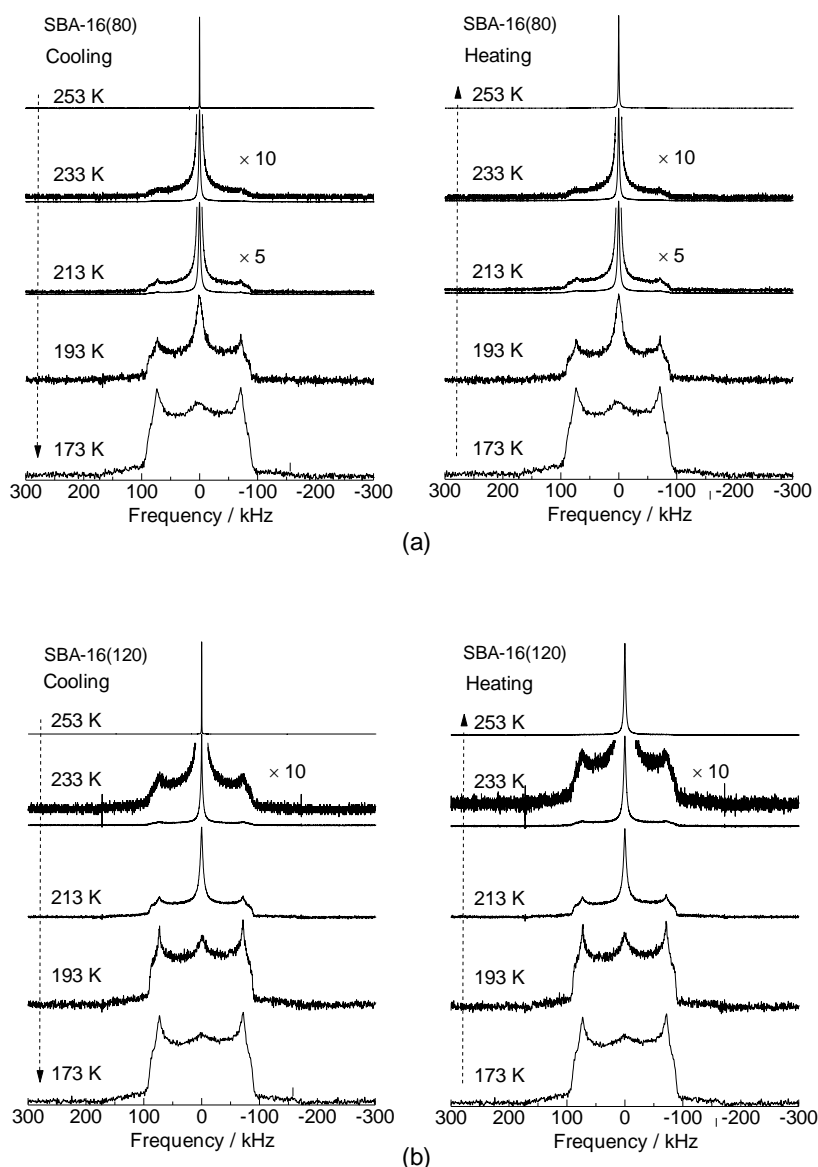


Figure 4-2 ²H NMR spectra of D₂O confined in (a) SBA-16(80) and (b) SBA-16(120) determined at decreasing and increasing temperatures. Spectra for other porous systems are given in Figure 4-3. Numbers near the curves are magnifications.

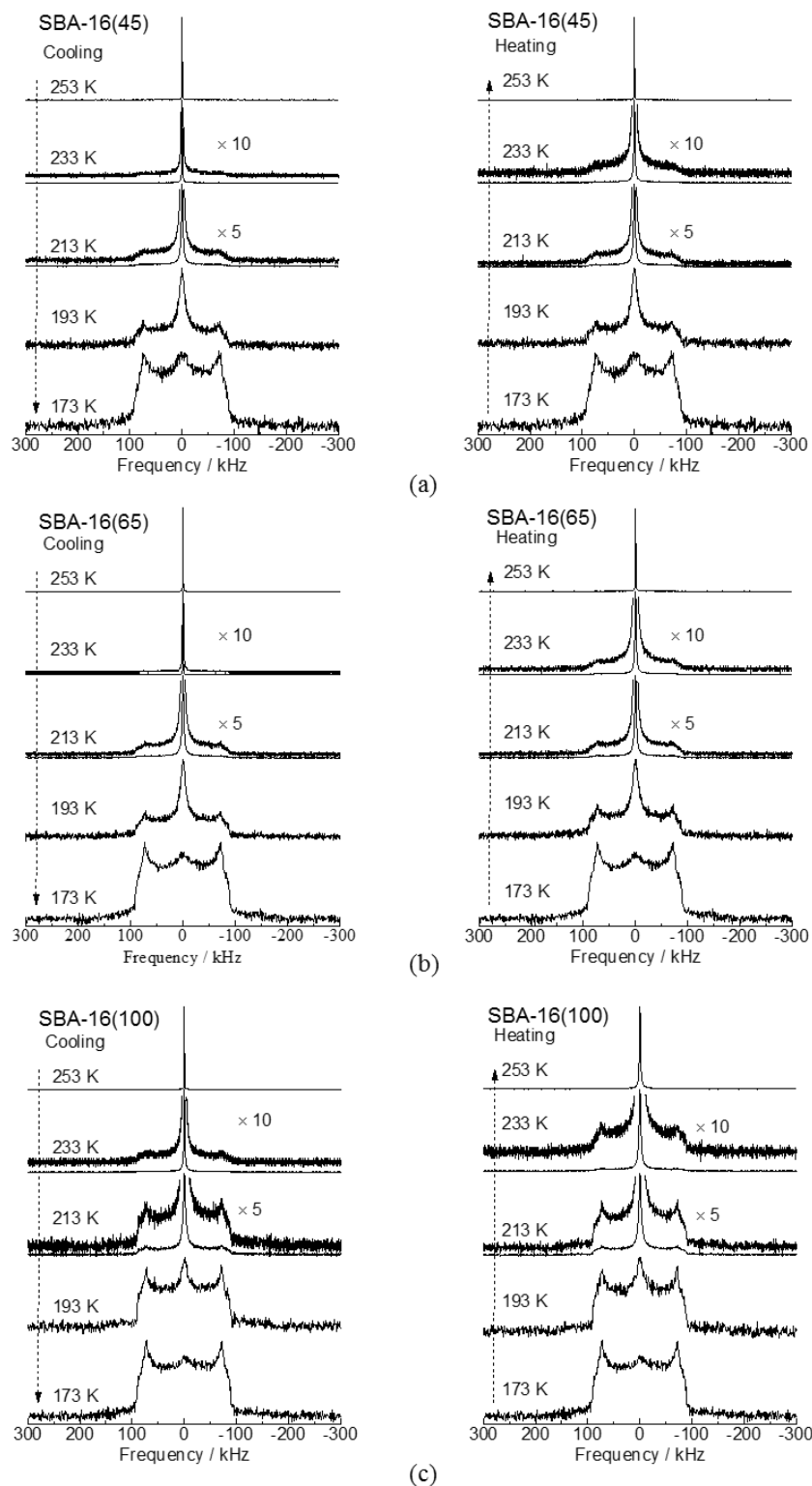


Figure 4-3 ^2H NMR spectra of D_2O confined in (a) SBA-16(45), (b) SBA-16(65), and (c) SBA-16(100).

For comparison, ^1H NMR was measured on the water confined in SBA-16(80), as shown in Figure 4-4. As temperature decreased, the sharp peak thickened. At 213 K, an additional broad peak appeared and grew, suggesting the occurrence of an immobile phase. The intensity of the sharp peak decreased, as found in the system with D_2O . As temperature was raised, the broad peak became thinner and a sharp peak emerged, as found in the system with D_2O .

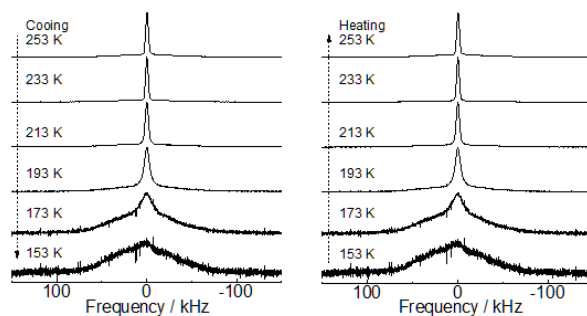


Figure 4-4 ^1H NMR spectra of H_2O confined in SBA-16(80) determined at decreasing and increasing temperatures.

In order to extract the change of signal of the liquid phase from the observed ^2H NMR spectra, a Lorentzian function was fitted to the sharp component of the spectrum while the contribution of the broad component $I(\omega)$ observed in the solid phase was calculated using Equation 3-7, Equation 3-8, Equation 3-9 by changing parameters, quadrupole constant e^2qQ/h , asymmetry parameter η and spin-spin relaxation time T_2 . One example for D_2O confined in SBA-16(80) is shown in Figure 4-5 (a).

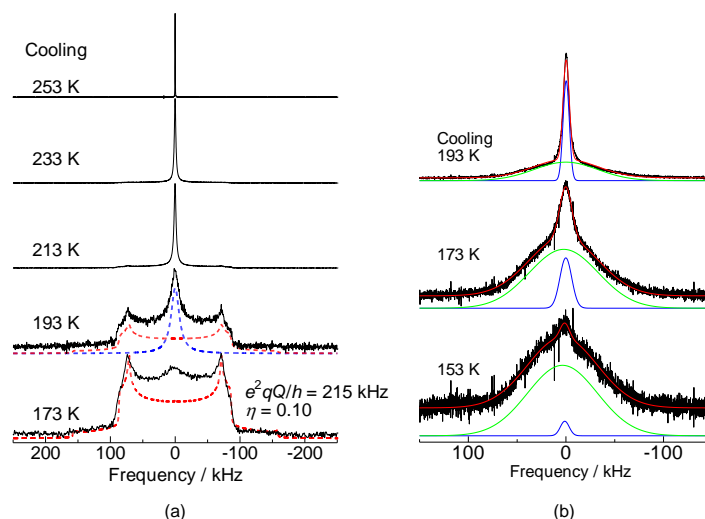


Figure 4-5 Deconvolution of NMR spectra water confined in SBA-16(80). (a) D_2O : Lorentzian function for sharp component and broad component due to quadrupole interaction. (b) H_2O : two Gaussian functions.

For the system with H₂O confined in SBA-16(80), two Gaussian fittings were performed on the experimental peak (Figure 4-5 (b)).

In Figure 4-6 (a), the relationship between peak area intensity of the liquid phase of D₂O versus temperature is shown for SBA-16(45) through SBA-16(120). A hysteresis loop is recognizable in each sample. The hysteresis loop is anticipated from the irreversible DSC peaks at corresponding temperatures for cooling and heating processes except for the D₂O system in SBA-16(100), in which NMR intensity decreases at somewhat higher temperatures than 235 K at which freezing of D₂O in the spherical pore occurs. In the case of D₂O in SBA-16(120), it is clearly shown that freezing starts at the outermost outlet of large interconnecting channels. The presence of a small amount of mesoporous channels in the hysteresis loop of adsorption isotherms of water causes some portions of water to begins to freeze spectroscopically [13]. The NMR intensity observed after the drop at around 235 K remained high and showed the presence of a significant amount of mobile phases, whose value decreased as micropore volume decreased; microporosity was estimated from the t-plot analysis of nitrogen adsorption in previous experiments [13]. The ratio of micropore adsorption to total adsorption of nitrogen is 0.468 for SBA-16(45), 0.462 for SBA-16(65), 0.366 for SBA-16(80), 0.317 for SBA-16(100), and 0.053 for SBA-16(120) (Figure 4-7). Thus the dynamic nature of D₂O in micropores decreased gradually then steeply below 210 K. This suggests that freezing leads to loose dynamic motions (derivatives are shown in Figure 4-6 (b)).

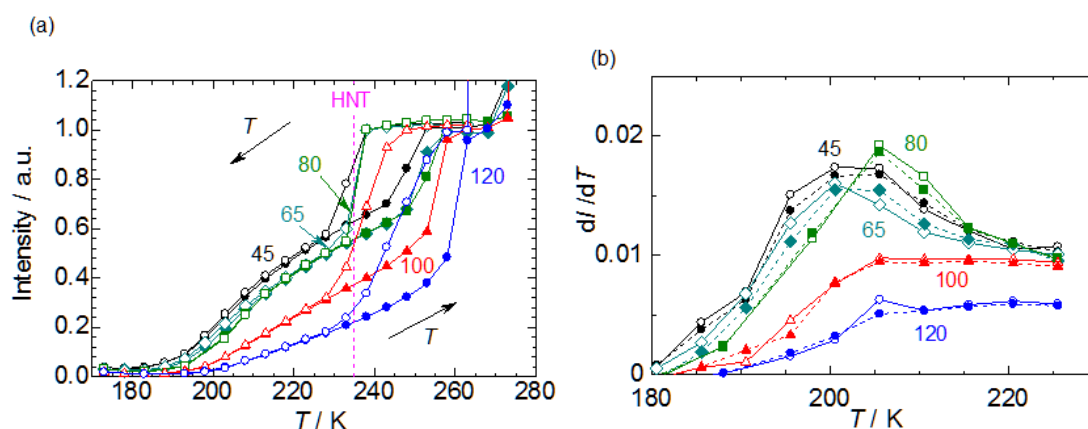


Figure 4-6 (a) Temperature change of area intensity of sharp component of ²H NMR spectra of D₂O confined in SBA-16. Numbers near the curves show the temperatures (°C) at which samples formed. HNT is the homogeneous nucleation temperature determined from DSC measurements. (b) shows the derivatives of the curves in the low temperature range of (a).

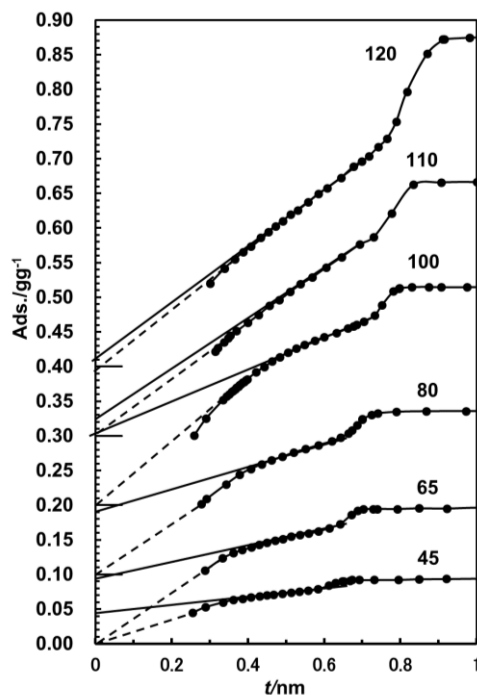


Figure 4-7 t-plot of adsorption isotherms of N_2 on SBA-16. The previously reported figure had a mistake on the abscissa, i.e., the t-value was half of the correct value. t-plot of adsorption isotherms of N_2 on SBA-16. t-value is a measure of pore radius [13].

When the system was heated, NMR intensity increased reversibly along a line of cooling and extended continuously until the temperature for melting of D_2O in the spherical pores. It is reasonable to assume that the dynamics of D_2O in the micropores are merged in the above phase.

Figure 4-8 compares the intensity-temperature curves for D_2O and H_2O confined in SBA-16(80). The intensity relation is apparently different between the two but the temperature for the occurrence of hysteresis corresponds to the difference (~ 4 K) in melting point for D_2O and H_2O in SBA-16 (Fig. 1 and Fig. 6b in ref. [13]). The difference in intensity relation is probably due to the lack of preciseness in deconvolution procedures on different line shapes for solid phases. It is reasonable to assume that the NMR studies using D_2O and H_2O observed here are similar.

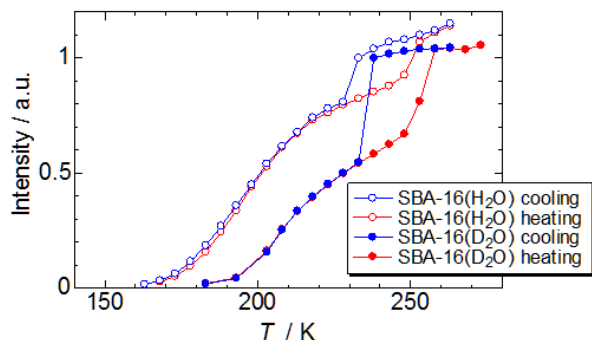


Figure 4-8 Comparison of temperature changes of peak area intensity of NMR spectra of D_2O and H_2O confined in SBA-16(80).

In order to obtain information on the dynamics of D₂O molecules, the temperature dependence of line-width was investigated. Full Width at Half Maximum (FWHM) values for the sharp component of the NMR spectrum for D₂O in SBA-16 were plotted in Figure 4-9. FWHM values were lowest at temperatures as low as 235 K and were almost constant, independent of the samples. In the case of D₂O in SBA-16(100) and SBA-16(120), FWHM increased sharply as temperature approached 235 K. The FWHM of other SBA-16 forms also increased simultaneously at 230 K. The difference between both groups may be attributed to the difference in size of the interconnecting channels. On the other hand, the difference in mobility at low temperatures is due to the difference in micropore size. From a previous N₂ adsorption experiment [13], micropore size was estimated to be 0.72 nm for SBA-16(45), 0.80 nm for SBA-16(65), 0.90 nm for SBA-16(80), 1.0 nm for SBA-16(100), and >1.0 nm for SBA-16(120) (Figure 4-7). Thus, larger freedom of water rotation in a larger pore is acceptable.

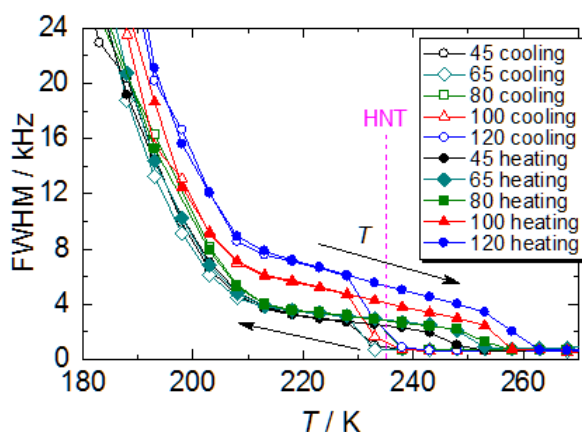


Figure 4-9 Temperature change of FWHM of sharp component of ²H NMR spectra of D₂O confined in SBA-16.

After spherical pore water freezes, FWHM increases, which is followed by a slow then a steep increase at 210 K. A sudden increase of FWHM indicates thorough freezing, vitrification or glass formation of water in a micropore [12, 16, 109].

When the sample is heated from a frozen state, FWHM decreases reversibly along a gradient of decreasing temperatures but suddenly drops at the temperature at which D₂O ice melts in spherical pores. That is, dynamics of micropore water is immersed in the spherical pore water dynamics.

3. Rotational correlation time obtained by ^2H NMR T_1

As another measure of the dynamics of water molecules, ^2H NMR spin-lattice relaxation time T_1 was measured for D_2O confined in SBA-16(80) (Figure 4-10) and T_1 for other SBA-16 samples are provided in Figure 4-11 (a)-(d). As temperature decreases from room temperature, T_1 decreases gradually and reaches a minimum at freezing temperature, after which it begins to increase. When temperature increases, T_1 passes the minimum reversibly, but runs below the plots observed at decreasing temperatures and forms a hysteresis loop to close at 253 K. The line of plots before the minimum observed at decreasing temperatures is due to D_2O confined in the spherical pores while the smooth line observed with increasing temperature is mainly due to D_2O in micropores. In this temperature range, T_1 is dominated by isotropic rotation of water molecule. The minimum T_1 values are larger than those calculated from the BPP equation [110] (Equation 3-12 and Equation 3-13) using the quadrupole interaction parameters of $e^2qQ/h = 215$ kHz and $\eta = 0.1$ which were obtained from the line shape of the ^2H NMR spectrum at low temperatures. These differences, which indicate the dynamic heterogeneity of water [111], are attributed to the coexistence of water confined in the various types of pores in SBA-16.

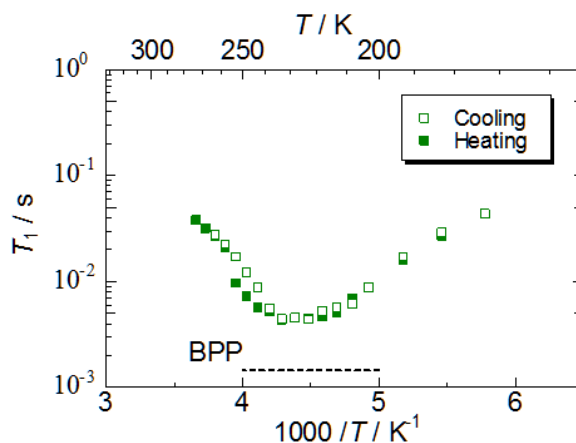


Figure 4-10 Temperature change of ^2H NMR T_1 for D_2O confined in SBA-16(80).

Broken line shows the minimum T_1 value calculated from the BPP equation.

By using the Cole–Cole distribution function (Equation 3-17) for the correlation time of isotropic rotation of water molecule, T_1 is written as Equation 3-12 and Equation 3-18. τ_{cc} and α_{cc} indicate the correlation time at the maximum position and the distribution width of correlation time, respectively. $\alpha_{cc}=1$ yields the case of a single correlation time and α_{cc} decreases as the distribution width of correlation time increases. Table 4-1 represents α_{cc} estimated from the minimum T_1 value. The α_{cc} of SBA-16(100) and SBA-16(120) was smaller than that of SBA-16(45), SBA-16(65) and SBA-16(80). Therefore, the dynamic

heterogeneity of water in SBA-16(100) and SBA-16(120) was higher than that in SBA-16(45), SBA-16(65) and SBA-16(80). These results are consistent with the large distribution of frozen temperature of pore water observed in DSC and the large freedom of mobility of pore water predicted from the FWHM of the ^2H NMR spectrum for SBA-16(100) and SBA-16(120).

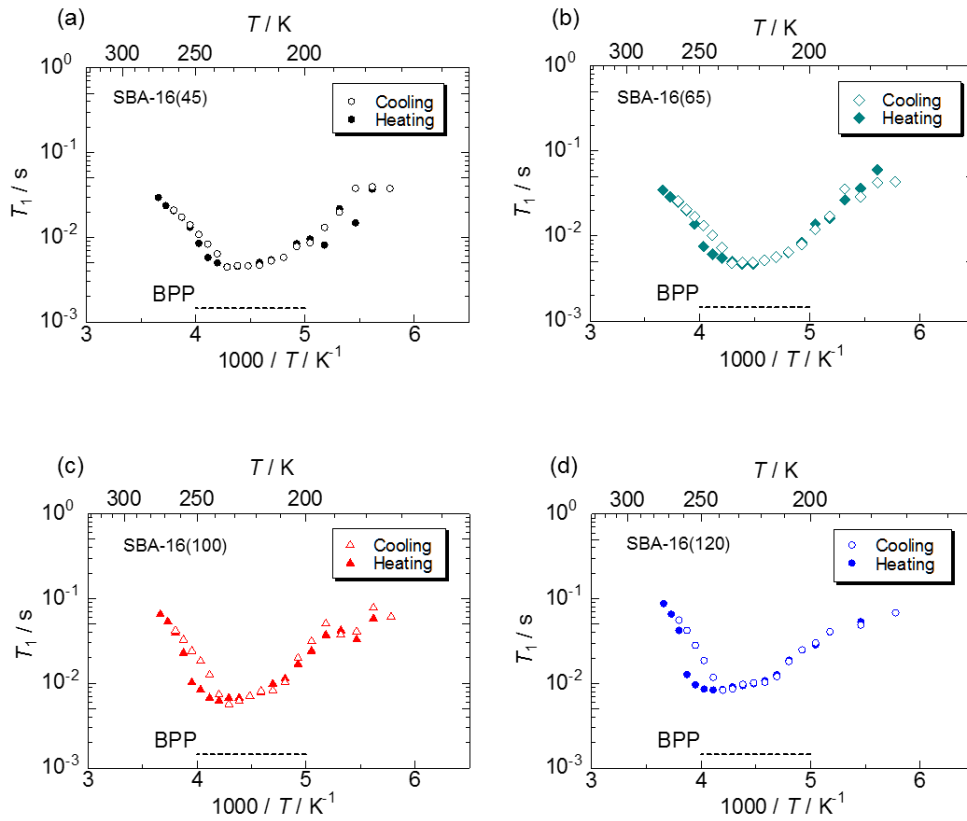


Figure 4-11 ^2H NMR T_1 of D_2O confined in (a) SBA-16(45), (b) SBA-16(65), (c) SBA-16(100) and (d) SBA-16(120).

Table 4-1 Distribution width α_{cc} of correlation time of water dynamics

	SBA-16(45)	SBA-16(65)	SBA-16(80)	SBA-16(100)	SBA-16(120)
α_{cc}	0.38	0.36	0.39	0.27	0.18

τ_{cc} was obtained from the T_1 values at each temperature using Equation 3-12, Equation 3-18 and the α_{cc} value estimated from the minimum T_1 value.

Figure 4-12 shows the correlation time for SBA-16(80) as a function of temperature inverse while values for other SBA-16 samples are given in Figure 4-13 (a)-(d). From room temperature to freezing temperature of D_2O in the spherical pores of SBA-16, the Vogel-

Fulcher-Tammann (VFT) relation (Equation 4-1)

$$\tau_{CC} = \tau_0 \exp\left(\frac{DT_0}{T - T_0}\right) \quad \text{Equation 4-1}$$

was fitted to the experimental correlation time. Here, D indicates deviation from the Arrhenius law. T_0 and τ_0 are vitrification temperature and temperature-independent constant, respectively. The parameters T_0 , τ_0 and D obtained from the fitting are presented in Table 4-2.

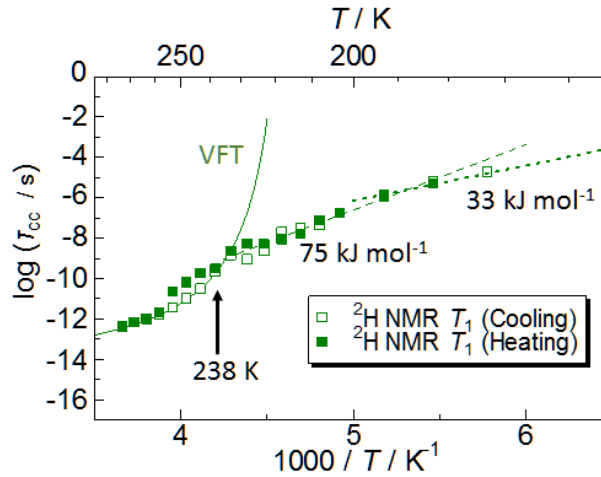


Figure 4-12 Correlation time of rotation of D₂O confined in SBA-16(80) obtained by ²H NMR T_1 as a function of temperature inverse. Solid line shows VFT fitting. Broken and dashed lines are Arrhenius fittings. The fitting parameters are shown in Table 4-2.

Table 4-2 Parameters for correlation time of water dynamics.

	SBA-16(45)	SBA-16(65)	SBA-16(80)	SBA-16(100)	SBA-16(120)
Arrhenius parameters					
Above 200 K					
τ_0 (s)	5.3×10^{-24}	1.2×10^{-26}	9.3×10^{-27}	1.6×10^{-33}	3.2×10^{-34}
E_a (kJ/mol)	63	74	75	107	114
Below 200 K					
τ_0 (s)	4.0×10^{-13}	9.0×10^{-13}	1.5×10^{-15}	1.5×10^{-11}	2.0×10^{-12}
E_a (kJ/mol)	25	25	33	25	33
VFT parameters					
τ_0 (s)	7.2×10^{-16}	1.1×10^{-15}	3.6×10^{-15}	2.6×10^{-17}	1.2×10^{-22}
D	2.8	2.1	1.3	1.4	3.8
T_0 (K)	193	200	212	217	211

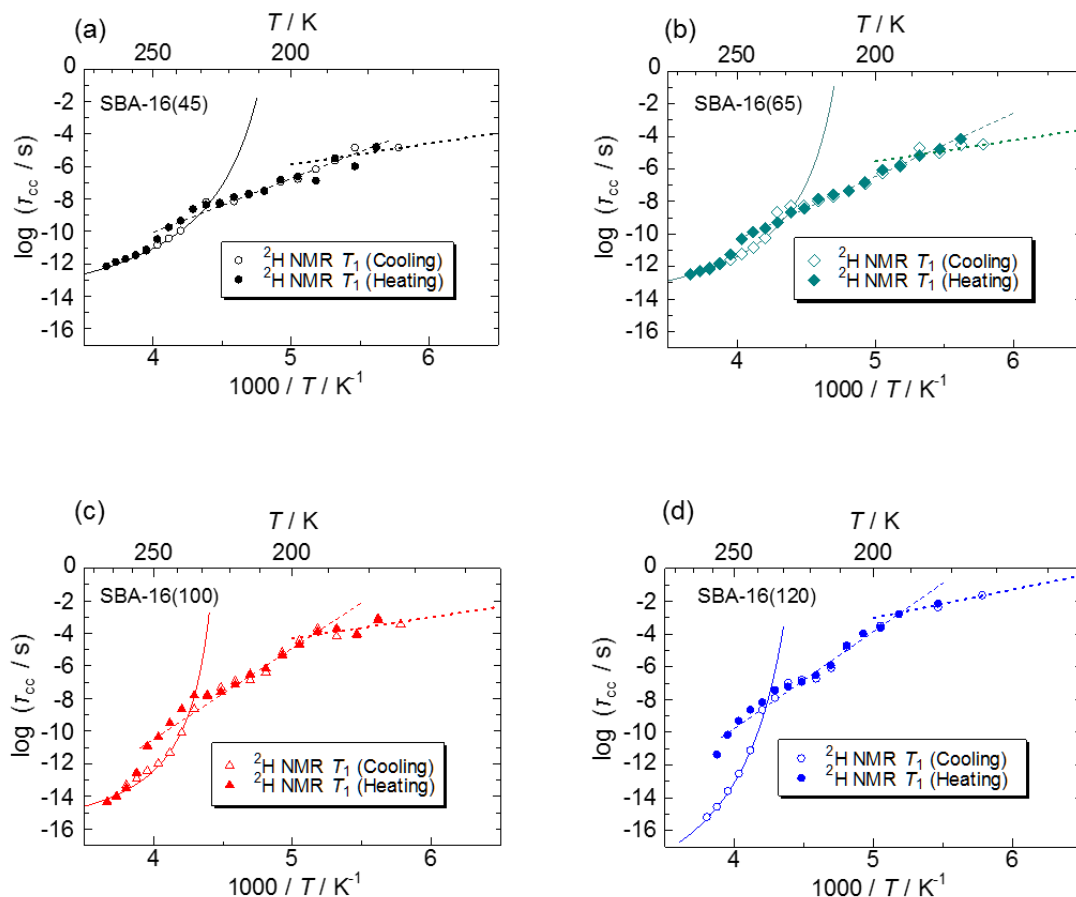


Figure 4-13 Correlation time of dynamics of D₂O confined in (a) SBA-16(45), (b) SBA-16(65), (c) SBA-16(100), (d) SBA-16(120) as a function of temperature inverse. Solid line shows VFT fitting. Broken and dashed lines are Arrhenius fittings. The fitting parameters are shown in Table 4-2 Parameters for correlation time of water

These parameters are comparable to those determined by neutron spin echo (NSE) measurements obtained in the Q range of 11.9-15.7 nm⁻¹ for SBA-16(80) in which vitrification temperature is 198.5±3.3 K, $\tau_0 = 0.30 \pm 0.17$ ps, and $D = 1.129 \pm 0.099$ [112].

In this temperature range, fragile water clusters before changing to strong water in the pores. In the NSE experiment, dynamic entities are D₂O clusters developed in the liquid D₂O and their growth in the liquid was assessed. On the other hand, ²H NMR T_1 showed the isotropic rotation of water molecules in the cluster. The consistency of parameters obtained by NSE and ²H NMR T_1 indicates that the growth of hydrogen bonds accompanied by the development of clusterization strongly affects the isotropic rotation of water molecules.

A linear relation observed below the freezing temperature of D₂O in SBA-16 is attributed to D₂O in micropores. Table 4-2 represents the pre-exponential factor τ_0 and the activation energy E_a obtained by fitting the Arrhenius relation. The obtained activation energies of the dynamic motion of D₂O in micropores above 200 K were much larger than ~ 23 kJmol⁻¹ found in ice I_h [113]. Furthermore, the obtained τ_0 were abnormally small. These large energy values are physically unacceptable for the activation energy of the rotation of a water molecule. A large activation energy value of ~ 74 kJmol⁻¹ was also obtained for water confined in silica matrices (MCM41 C10) with a pore diameter of 2.1 nm above 180 K by dielectric spectroscopy and was interpreted as non-Arrhenius behavior before the fragile- strong transition [114]. Water in small pores less than ~ 2.1 nm does not form crystalline ice [16]. FWHM of the ²H NMR spectrum indicates that the vitrification or glass formation of water in a micropore occurred suddenly at around 200 K. The non-Arrhenius behavior of the correlation time above 200 K in SBA-16 suggests that the growth of reinforced hydrogen bonds before creating a low density structure like ice without crystallization strongly affects the rotation of water in micropores.

The activation energy value obtained above 200 K increased with increasing pore size which reflects the larger freedom of cluster formation and water rotation in a larger pore.

Another linear relationship below 200 K presents an activation energy of 25~33 kJmol⁻¹ which is closer to that for the ice I_h . It is believed that the dynamics of vitrified water may be observed in this low temperature phase.

4. Conclusion

The dynamic properties of pore water in SBA-16 were studied by solid ²H NMR and ¹H NMR measurements as a function of pore size. Water in characteristic spherical pores of SBA-16 is characterized by freezing at the homogeneous nucleation temperature of water. From room temperature to freezing temperature, the correlation time of the isotropic rotation of water in the pores of SBA-16 followed a VFT relation. The formation and growth of clusters of fragile water that change to strong water affect the isotropic rotation of water in the pores. The vitrification of water in micropores takes place at around 200 K. Above 200 K, the correlation time of the rotation of water in micropores exhibited non-Arrhenius behavior. The growth of a cluster occurs gradually for water in micropores before vitrification. The rotation of water in micropores is strongly affected by the growth of a hydrogen bond before forming low density noncrystalline ice in this temperature range. The freedom of cluster formation and water rotation increased with increasing pore size.

Chapter 5 Sodium chloride aqueous solution confined with mesoporous silica SBA-16

Thermodynamic and dynamic properties of sodium chloride aqueous solution confined with mesoporous silica glass SBA-16 were investigated by DSC, ^2H NMR spectrum and ^2H and ^{23}Na NMR spin-lattice relaxation time (T_1) as a function of salt concentration. SBA-16 possesses the main spherical pores, interconnecting channels and micropores (corona). In the low concentration range, the generation of ice in spherical pores occurred at nearly homogeneous nucleation temperature (HNT) of bulk aqueous solution. As increasing concentration, the generation of ice in spherical mesopore disappeared. In the high concentration, the solution confined with spherical mesopore and micropore simultaneously froze at 190 K. This freeze temperature of solution in spherical mesopore was lower than HNT of bulk aqueous solution. Therefore, aqueous solution confined with mesopore may undergo rather vitrification than crystallization. Rotational correlation time of water in SBA-16 exhibited some variability. The correlation time of reconfiguration of water near sodium cation was nearly single. The width of distribution of correlation time decreased with increasing concentration. The correlation time of the isotropic rotation of water in the pores of SBA-16 followed Arrhenius behaviour above 190 K. Activation energy of water rotation near sodium cation (35-41 kJ/mol) was lower than that of water far sodium cation (50-56 kJ/mol).

1. Salts concentration inside pore obtained by NMR signal intensity

The NMR signal intensity is proportional to number of nucleus in sample. Thus, it is possible to obtain the abundance ratio of molecule or ion by using the ratio of the NMR signal intensity. By using prepared standard curve (Figure 2-2), the abundance ratio of sodium cation to deuterated water molecule in SBA-16 ($N_{\text{Na}}/N_{\text{D}_2\text{O}}$) was obtained from the ratio of ^{23}Na NMR signal intensity to ^2H NMR signal intensity ($I_{\text{Na}}/I_{\text{D}}$). $N_{\text{Na}}/N_{\text{D}_2\text{O}}$ in SBA-16 is listed in Table 5-1. Concentration of sodium chloride at sample preparation was not completely consistent with $N_{\text{Na}}/N_{\text{D}_2\text{O}}$. The evaporation of water at sample preparation might cause this mismatch. Figure 5-1 shows the plot of $N_{\text{Na}}/N_{\text{D}_2\text{O}}$ in SBA-16 vs. $N_{\text{Na}}/N_{\text{D}_2\text{O}}$ in sample tube whole. The $N_{\text{Na}}/N_{\text{D}_2\text{O}}$ in sample tube whole contained the contribution from excess solution in sample tube. In the case of 0.5-2.0 M sample, the $N_{\text{Na}}/N_{\text{D}_2\text{O}}$ in SBA-16 was larger than the $N_{\text{Na}}/N_{\text{D}_2\text{O}}$ in sample tube whole. This suggest that the solution is concentrated in the pores of SBA-16 because sodium cation is affinitive to a silica surface. In the case of 4.0 M sample, the $N_{\text{Na}}/N_{\text{D}_2\text{O}}$ in SBA-16 was almost same as the

$N_{\text{Na}}/N_{\text{D}_2\text{O}}$ in sample tube whole.

Table 5-1 Number ratio of sodium cation divided by deuterated water molecule ($N_{\text{Na}}/N_{\text{D}_2\text{O}}$) inside the pore of SBA-16. This was obtained from the NMR measurements at 238 K.

Concentration(M) of the solution at sample preparation	$N_{\text{Na}}/N_{\text{D}_2\text{O}}$ inside the pore
0.5	0.0242 ± 0.0012
1.0	0.0470 ± 0.0006
2.0	0.0674 ± 0.0005
4.0	0.0882 ± 0.0078

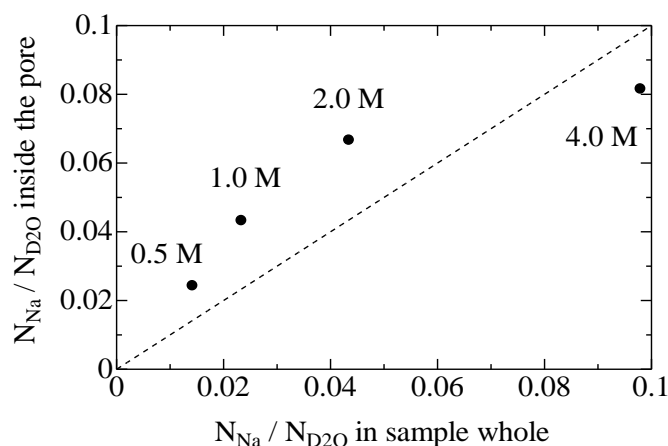


Figure 5-1 Vertical: Number ratio of sodium cation divided by deuterated water molecule ($N_{\text{Na}}/N_{\text{D}_2\text{O}}$) inside the pore of SBA-16. This was obtained from the NMR measurements at 238 K. Horizontal: $N_{\text{Na}}/N_{\text{D}_2\text{O}}$ in sample whole. This was obtained from the NMR measurements at room temperature. Broken line show that vertical value is same as horizontal value.

2. DSC analysis of sodium chloride aqueous solution confined with SBA-16

Figure 5-2 shows the DSC curves of deuterated sodium chloride aqueous solution confined with SBA-16. The DSC curve as decreasing temperature is shown Figure 5-2 (a). The first exothermic peak appeared at around 263 K in 0 M sample, at around 238 K in 0.1-5.0 M sample. This is ascribed to the freezing of external solution. A second exothermic peak appeared at 230-220 K in 0.0-2.0 M samples, dependently of salt concentration. This is due to the partially freezing of water in solution confined with the spherical mesopore, which is indicated by fp (freeze point) in the figure. This exothermic peak shifted to a low temperature and broadened at increasing salt concentration, and

disappeared in 3.0-5.0 M samples. A third exothermic peak appeared at 160-190 K in 0.3-5.0 M sample, independently of salt concentration. This is ascribed to the complete freeze of residual solution confined with SBA-16, which is indicated by ep (eutectic point) in the figure. The DSC curve as increasing temperature is shown Figure 5-2 (b). A first endothermic appeared at around 170 K in 0.3-5.0 M samples, which is indicated by ep in the figure. This endothermic peak was complicated and not clear. A second endothermic peak appeared at around 230 K in 0.5-1.0 M samples. This is ascribed to the partial melting of solution in the pore. The endothermic peak corresponding to complete melting of solution in the pore appeared at 238-250 K (indicated by mp (melt point)), dependently of salt concentration. Frozen solution in the pore melts at fairly higher temperatures than freezing temperature, and the melting temperature increases as salt concentration increases. Finally, external frozen solution melts above 250 K. In the following sections, the signature samples (0.5 M, 1.0 M, 2.0 M, 4.0 M) was investigated in more detail by NMR.

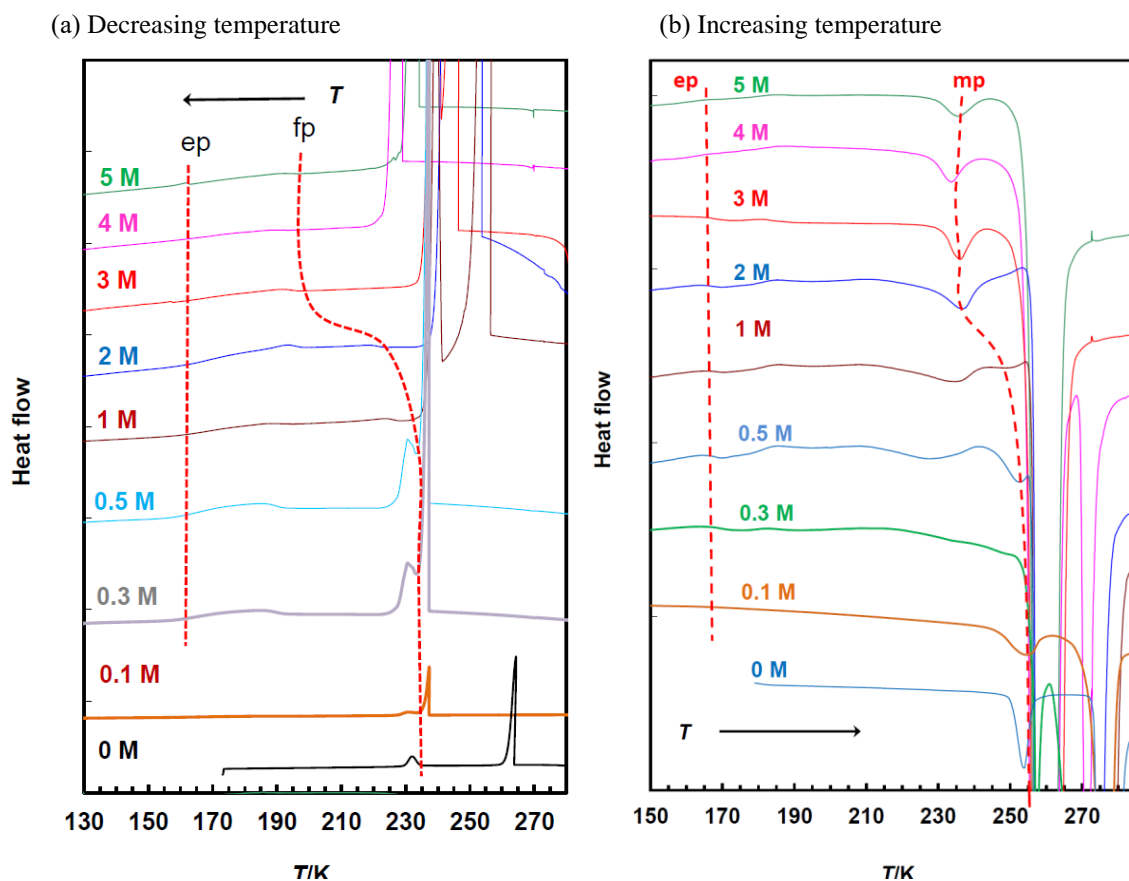


Figure 5-2 DSC curves of deuterated sodium chloride aqueous solution confined with SBA-16. Numbers near the curves show the salt concentration of prepared sample. Scanning speed for increasing and decreasing temperature is 5 Kmin^{-1} . fp and mp show the freezing and melting temperature of solution confined with SBA-16. ep shows the eutectic temperature of solution confined with SBA-16.

3. ^2H NMR spectrum of sodium chloride aqueous solution confined with SBA-16

Figure 5-3 (a), (b) shows the partially relaxed ^2H NMR spectra for deuterated (a) 0.5 M, (b) 4.0 M sodium chloride aqueous solution confined with SBA-16, respectively. The ^2H NMR line-shape was fitted by the two component model. One was the sharp component. The sharp component was fitted by using Lorentz function. It was thought that the sharp component derived from water with liquid-state in the pore. Other was the broad component. The line-shape of the broad component was powder pattern due to nuclear quadrupole interaction. The fitting parameter was $e^2qQ/h = 215$ kHz, $\eta = 0.10$. This line-shape means that molecular reorientation is much slower than quadrupole interaction. Thus, the broad component derived from water with solid-state in the pore. The spectra for other concentration systems (1.0 M, 2.0 M) are given in Figure 5-4.

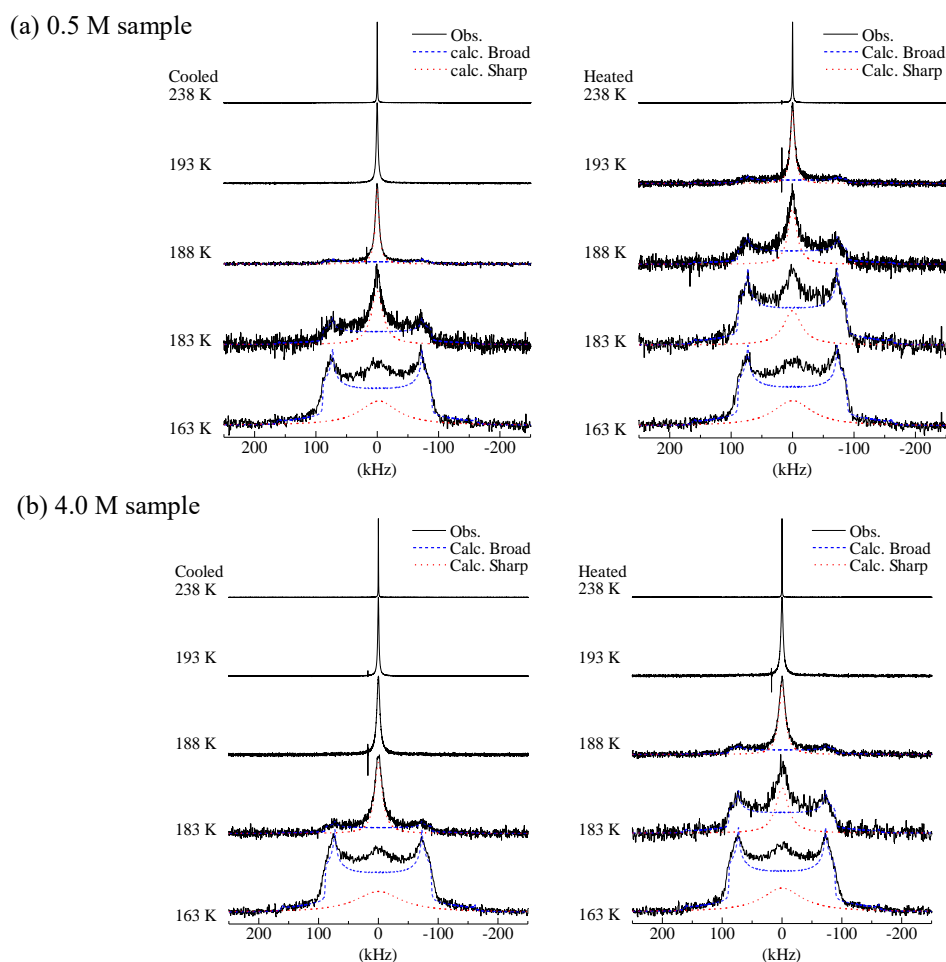


Figure 5-3 The partially relaxed ^2H NMR spectra for (a) 0.5 M, (b) 4.0 M deuterated sodium chloride aqueous solution confined with SBA-16. The solid line shows the observed spectra. The blue broken and red dotted line show the calculated spectra of sharp component and broad component, respectively. The spectra for other concentration systems are given in Figure 5-4.

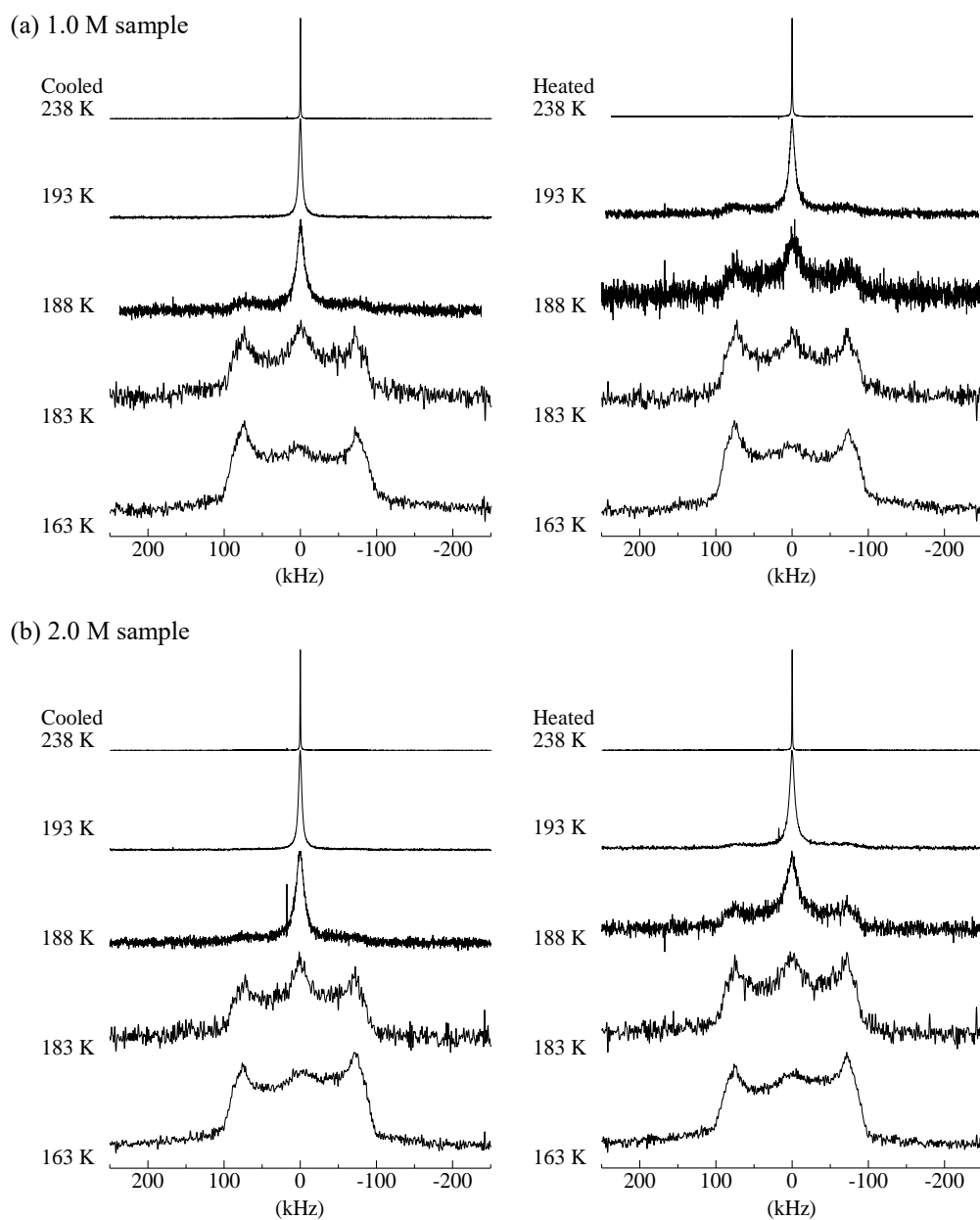


Figure 5-4 The partially relaxed ^2H NMR spectra for (a) 1.0 M, (b) 2.0 M deuterated sodium chloride aqueous solution confined with SBA-16.

Figure 5-5 (a) shows the temperature dependence of signal intensity of sharp component obtained by fitting ^2H NMR spectra for deuterated 0.0-4.0 M sodium chloride aqueous solution confined with SBA-16. The signal intensity was normalized by the signal intensity at 238 K. In the case of 0.0 M (heavy water) sample, the freeze of water in the spherical mesopore occurred at around 235 K, which was close to HNT (232 K) of bulk pure water [13]. The hysteresis loop of 0.0 M sample was observed between 235K and 258 K, which is freeze and melt of water in spherical mesopore. The two horizontal

broken line in Figure 5-5 (a) shows the water ratio of the spherical mesopore, the inter-connecting channel and the corona-like micropore obtained by measurement for 0.0 M (heavy water) sample. In the case of salts samples, the hysteresis loop was observed in broader temperature ranges. This hysteresis loop was analogically attributed to freeze and melt of solution in spherical pore. To make this hysteresis clear, the difference of signal intensity between cooled and heated measurements is shown in Figure 5-5 (b). In the case of 0.5 M sample, the rapid drop of the signal intensity was observed at around 228 K. It was thought that this drop derived from the generation of pure ice inside spherical mesopore. The generation of ice in spherical pores occurred at nearly HNT of bulk aqueous solution [61]. The residual water in the pore froze at near 190 K. This is corresponding to results of DSC (Figure 5-2). In the case of 1.0 M sample, the drop of the intensity was much broader than that of 0.5 M sample, and moved to a lower temperature. This lower temperature shift derived from HNT shift due to adding salts [61]. In the case of 1.0 M samples, the cluster of water in the pore may not be large enough for an ice crystallite to grow from the smallest embryo stage of ~ 4.0 nm [10, 34]. Therefore, the phase separation of aqueous solution may be prevented by the confinement. In the case of 2.0-4.0 M samples, this drop was not observed above 190 K. This suggested that the generation of pure ice was impossible in the case of 2.0-4.0 M samples. The solution whole (sodium chloride and water) frozen simultaneously near 190 K. This freeze temperature of aqueous solution in the pore was lower than HNT of bulk aqueous solution [61]. Recently, L. Zhao et. al. reported that the confinement induces the vitrification of sodium chloride aqueous solution [56]. This freeze of water rotation may be more like a vitrification than a crystallization.

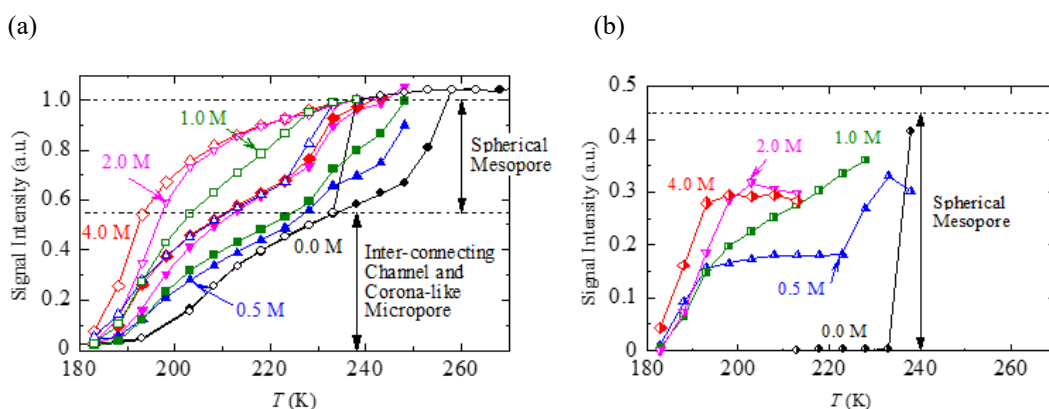


Figure 5-5 (a) Temperature dependence of ^2H NMR signal intensity of sharp component for deuterated 0.0-4.0 M sodium chloride aqueous solution confined with SBA-16. The signal intensity was normalized by the signal intensity at 238 K. The horizontal broken line shows ratio of the spherical mesopore, the inter-connecting channel and corona-like micropore obtained by measurement for 0.0 M (heavy water) sample. (b) Difference between cooled and heated measurements of (a).

Figure 5-6 shows the temperature dependence of signal intensity of broad component. Additionally, the sharp component shown in Figure 5-5 is shown again. The horizontal dotted line in the figure shows the fraction of micropore obtained by N₂ adsorptions. The fraction of micropore obtained by N₂ adsorptions was consistent with the fraction of broad component at 163 K. Hence, broad component observed below 190 K was assigned with water in micropore. The signal intensity of broad component increased with decreasing the sharp component at around 190 K. It was thought that the slowing down of molecular motion changed the sharp component to the broad component. Compared to pure heavy water (0.0 M), the vitrification temperature of water in micropore was decreased by about 10 K. At around 190 K, the sharp component and broad component coexisted. The wide distribution of rate of molecular reorientation shows the coexistence of slow and fast motion limit line-shape in ²H NMR spectrum. So, it was thought that the reorientation of water in micropore had some variability.

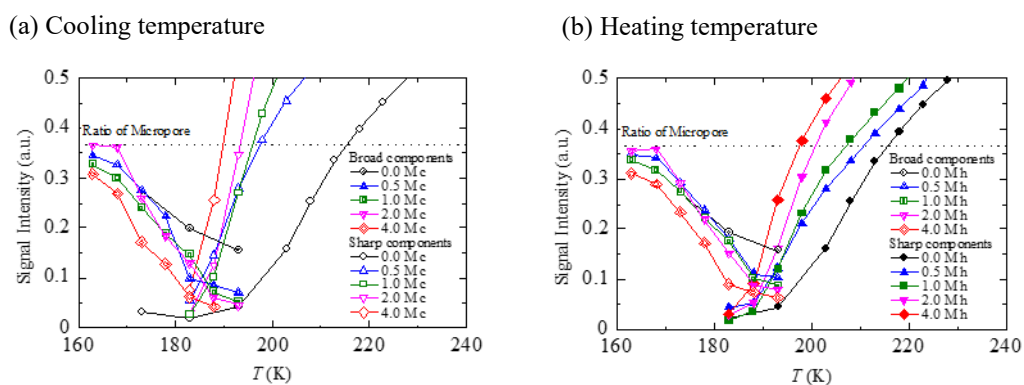


Figure 5-6 Temperature dependence of ²H NMR signal intensity of broad components for deuterated 0.0-4.0 M sodium chloride aqueous solution confined with SBA-16. Additionally, the sharp component shown in Figure 5-5 is shown again. The horizontal dotted line shows the fraction of micropore obtained by N₂ adsorptions.

Figure 5-7 shows the temperature dependence of full width at half maximum (FWHM) of sharp component for deuterated 0.0-4.0 M sodium chloride aqueous solution confined with SBA-16. The FWHM can be related to mobility of water with liquid-state. With increasing mobility of water, the FWHM decrease. In the case of 0.5-4.0 M sample, the FWHM rapidly increased with decreasing temperature below around 200 K. The concentration dependence of the FWHM was not large within 0.5 M to 4.0 M, because the sharp component did not involve the contribution from water with solid-state in the

pore. The FWHM below 223 K at heated measurement was derived from water in micropore. Compared with the case of 0.0 M (heavy water) sample, the FWHM was much smaller below around 223 K. Adding the salt made mobility of water in micropore much higher. In the case of 0.0 M (heavy water) sample, the large FWHM was derived from the large variability of water dynamics. Adding the salt decreased the freedom of water rotation. In other words, the dynamic heterogeneity of water in micropore decreased as adding salt.

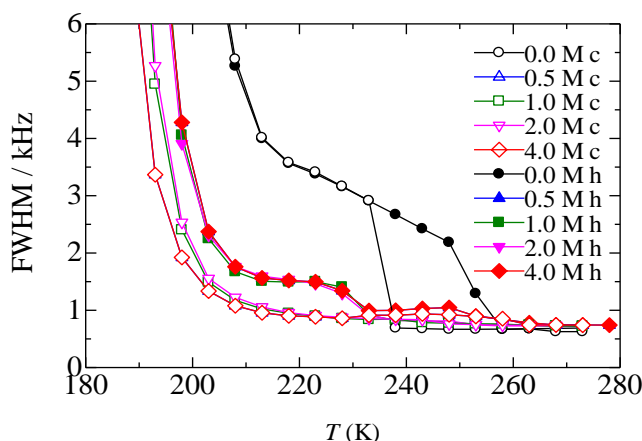


Figure 5-7 Temperature dependence of full width at half maximum (FWHM) of sharp component for deuterated 0.0-4.0 M sodium chloride aqueous solution confined with SBA-16. The 0.0 M (heavy water) data already has been shown once in Chapter 4.

4. Rotational correlation time obtained by NMR T_1

Figure 5-8 (a), (b) shows the temperature dependence of ^2H NMR T_1 for (a) 0.5 M, (b) 4.0 M deuterated sodium chloride aqueous solution confined with SBA-16, respectively. The vertical solid and dotted line shows the freezing temperature of water in spherical pore obtained from ^2H NMR intensity and DSC. In the case of 0.5 M sample, a part of water in spherical mesopore froze at around 228 K (solid line). The residual solution in spherical mesopore froze at 190 K (dotted line). In the case of 4.0 M sample, the solution in spherical mesopore froze at around 190 K (dotted line). The concentration dependence of ^2H NMR T_1 below 228 K was not large within 0.5 M to 4.0 M, because ^2H NMR T_1 was obtained from only the fast relaxation component and did not involve the contribution from the ice freezing completely in the pore. The ^2H NMR T_1 of both samples was minimum value at around 200 K. The ^2H NMR T_1 is predicted to be dominated by the isotropic rotation of water molecules above 190 K. For the isotropic rotation of water

molecules, ^2H NMR T_1 is written as Equation 3-12. In the case of single correlation time (No distribution), Equation 3-13 is used. The minimum value of ^2H NMR T_1 was estimated to be 1.5×10^{-3} s from Equation 3-12 and Equation 3-13 using the quadrupole interaction parameters of $e^2qQ/h = 215$ kHz and $\eta = 0.10$ which were obtained from the line shape of the ^2H NMR spectrum at low temperatures. The dot-and-dash line in the figure shows this theoretical minimum value. The observed T_1 minimum (2.9×10^{-3}) was longer than theoretical value. This result suggests the distribution of the correlation time τ . In the case of symmetrical Cole-Cole distribution of correlation time, Equation 3-18 is used. From the minimum of ^2H NMR T_1 for 0.5 M sample, $\alpha_{cc}=0.46$ was estimated. In a similar way, $\alpha_{cc}=0.57$ was estimated at 4.0 M sample. The width of distribution at 4.0 M sample was smaller than that at 0.5 M sample. In the case of 0.0 M (heavy water), $\alpha_{cc}=0.39$ was maintained in Chapter 4. It was thought that the sodium cation canceled the variability of correlation time generated by the interaction silica surface.

Figure 5-9 (a), (b) shows the temperature dependence of ^{23}Na NMR T_1 for (a) 0.5 M (b) 4.0 M deuterated sodium chloride aqueous solution confined with SBA-16, respectively. The longitudinal relaxation was fitted by single exponential function at all temperature. The ^{23}Na NMR T_1 of both samples was minimum value at around 210 K. The ^{23}Na NMR T_1 is predicted to be dominated by reconfiguration of water near sodium cation above 190 K. Then, the ^{23}Na NMR T_1 is written as Equation 3-15. The minimum value of ^{23}Na NMR T_1 was estimated to be 3.1×10^{-4} s from Equation 3-15 and Equation 3-13 using the quadrupole interaction parameters of $e^2qQ/h = 1083$ kHz and $\eta = 0.77$ which were obtained from the ^{23}Na NMR of $\text{NaCl} \cdot \text{D}_2\text{O}$ crystal [106]. These parameters were agreed with magnitude of isotropic quadrupolar shift in our ^{23}Na NMR (See Figure A1 in Appendix). The observed T_1 minimum (4.4×10^{-4} s) was slightly longer than this theoretical value. In a manner analogous to ^2H NMR T_1 , the width of distribution of correlation time was obtained. From the minimum of ^{23}Na NMR T_1 for 0.5 M sample, $\alpha_{cc}=0.91$ was estimated. In a similar way, $\alpha_{cc}=0.76$ was estimated at 4.0 M sample. The width of distribution obtained from ^{23}Na NMR T_1 was small, nearly single correlation time unlike the case of ^2H NMR T_1 . Water near sodium cation did not have the dynamic heterogeneity. This fact was consistent with the smaller dynamic heterogeneity of water observed by ^2H NMR FWHM and ^2H NMR T_1 as adding salt.

Figure 5-10 shows the temperature dependence of rotational correlation time obtained by ^2H NMR T_1 . The solid red and broken blue lines show Arrhenius fit of correlation time at heating and cooling measurement, respectively. The activation energy obtained by ^2H NMR T_1 is shown near fitted line, respectively. In the case of 0.0 M (heavy water), it was showed that correlation time of water in spherical mesopore above 238 K showed Vogel-

Fulcher-Tammann relation because of the growth of hydrogen bonding network with decreasing temperature. In the case of the salt solution, the correlation time above 190 K showed Arrhenius behavior. The reason why is that sodium cation prevents the growth of hydrogen bonding network of water. In the case of the 0.5 M sample, a part of solution in spherical mesopore and the solution in micropore were liquid-state between 228 K (solid line) and 190 K (dotted line) at cooling measurement. The activation energy of rotation of this water in the pore of SBA-16 was 56 kJ/mol. In the case of the 4.0 M salt solution, the activation energy of water rotation in the pore of SBA-16 was 50 kJ/mol. The activation energy of water rotation decreased slightly with increasing salt concentration. At heating measurement, only water in micropore was observed below 228 K. In the case of the 0.5 M salt solution, the activation energy of water rotation in the micropore of SBA-16 obtained by ^2H NMR T_1 was 76 kJ/mol. This value was comparable in magnitude to the value 75 kJ/mol observed in the case of 0.0 M (heavy water) in micropore of SBA-16. The activation energy of water dynamics in micropore were much larger than that in the spherical mesopore. Molecular rotation of water in micropore was restricted more compared to water in the spherical mesopore. This large activation energy was interpreted as non-Arrhenius behavior before the fragile-strong transition in the case of pure heavy water (0.0 M) in SBA-16. In the case of 0.5 M, dynamics of water in the micropore behaved similarly to the case of pure heavy water (0.0 M). In the case of the 4.0 M sample, the activation energy of water rotation in the micropore was 64 kJ/mol. The activation energy of water rotation in the micropore decreased slightly with increasing salt concentration similar to water in the spherical mesopore.

Figure 5-11 shows the temperature dependence of correlation time of the reconfiguration of water near sodium cation obtained by ^{23}Na NMR T_1 . The solid blue lines show Arrhenius fit of correlation time at cooling measurement. The activation energy obtained by ^{23}Na NMR T_1 is shown near fitted line, respectively. In the case of the 0.5 M salt solution, the activation energy of water reconfiguration near sodium cation in the mesopore of SBA-16 obtained by ^{23}Na NMR T_1 was 35 kJ/mol. In the case of the 4.0 M salt solution, the activation energy was 41 kJ/mol. The activation values of water reconfiguration obtained by ^{23}Na NMR T_1 were smaller than that of water rotation in the pore obtained by ^2H NMR T_1 . The activation energy of water reconfiguration near sodium cation increased slightly with increasing salt concentration. However, the concentration dependence of the activation energy was small.

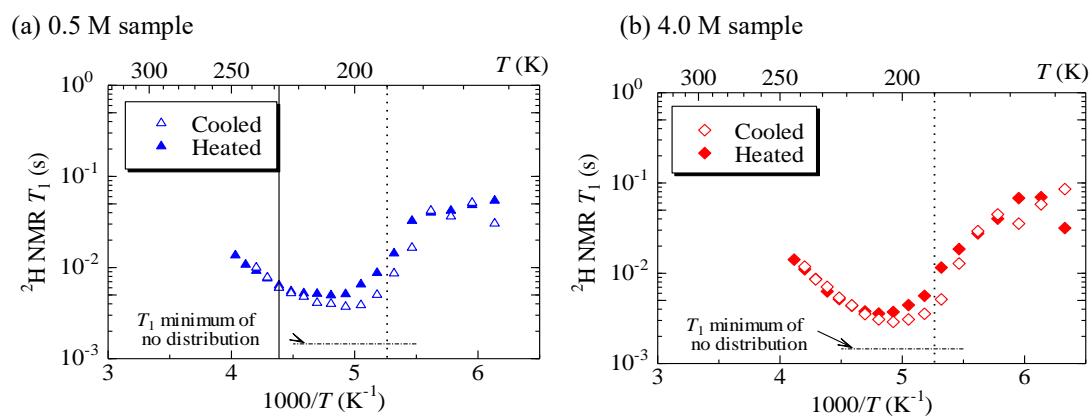


Figure 5-8 Temperature dependence of ^2H NMR T_1 for (a) 0.5 M (b) 4.0 M deuterated sodium chloride aqueous solution confined with SBA-16. The vertical solid and dotted line shows the freezing temperature of water in spherical pore obtained from ^2H NMR intensity and DSC. The dot-and-dash line shows the theoretical minimum in the case of single correlation time.

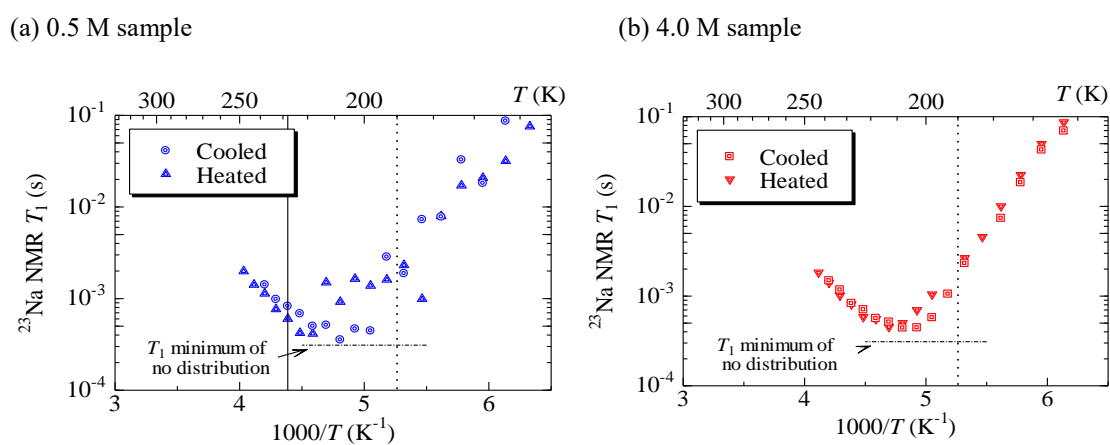


Figure 5-9 Temperature dependence of ^{23}Na NMR T_1 for (a) 0.5 M (b) 4.0 M deuterated sodium chloride aqueous solution confined with SBA-16. The vertical solid and dotted line shows the freezing temperature of water in spherical pore obtained from ^2H NMR intensity and DSC. The dot-and-dash line shows the theoretical minimum in the case of single correlation time.

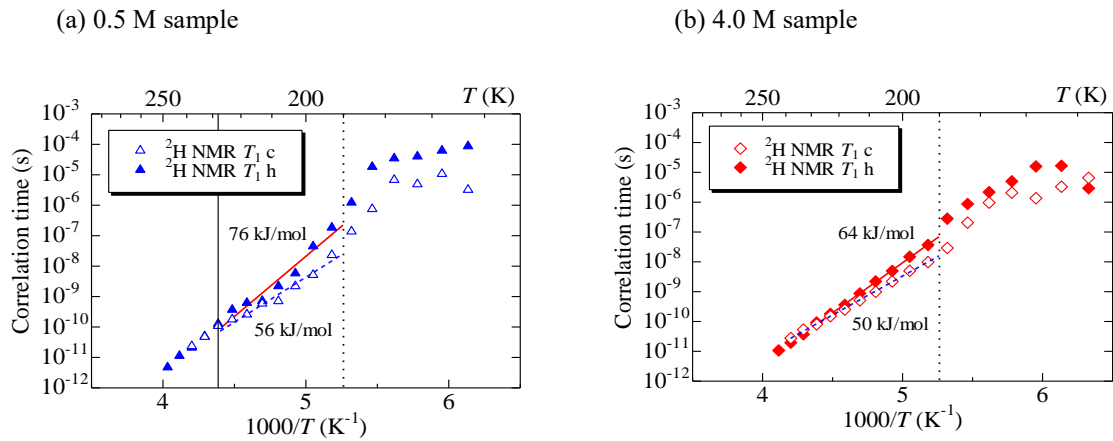


Figure 5-10 Temperature dependence of rotational correlation time obtained by ^2H NMR. (a) and (b) show 0.5 M and 4.0 M deuterated sodium chloride solution confined with SBA-16, respectively. The vertical solid and dotted line shows the freezing temperature of water in spherical pore obtained from ^2H NMR intensity and DSC. The solid red and broken blue lines show Arrhenius fit of correlation time at heating and cooling measurement, respectively. The activation energy obtained were shown near fitted line, respectively.

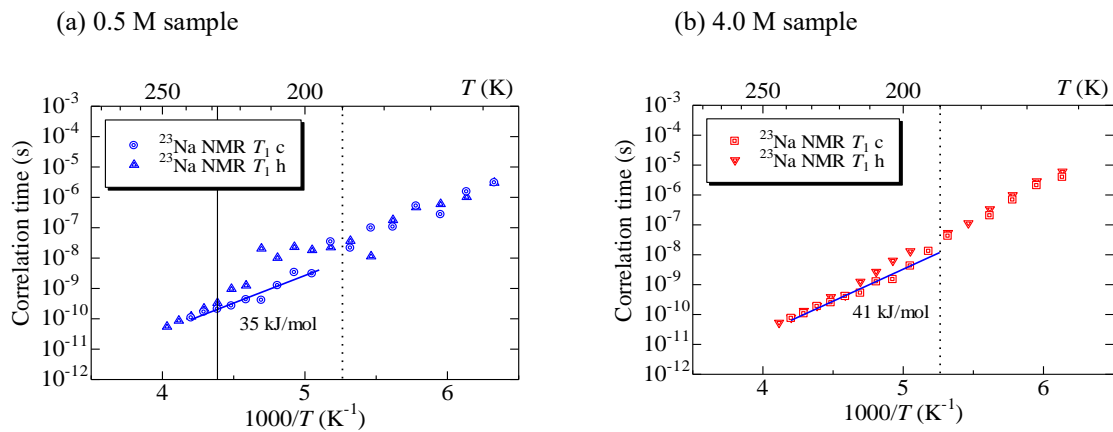


Figure 5-11 Temperature dependence of rotational correlation time obtained by ^{23}Na NMR. (a) and (b) show 0.5 M and 4.0 M deuterated sodium chloride solution confined with SBA-16, respectively. The vertical solid and dotted line shows the freezing temperature of water in spherical pore obtained from ^2H NMR intensity and DSC. The solid blue line shows Arrhenius fit of correlation time at cooling measurement. The activation energy obtained were shown near fitted line.

5. Conclusion

The freezing and melting temperature of sodium chloride aqueous solution confined with SBA-16 was investigated by DSC and ^2H NMR spectrum as a function of concentration. In the low concentration range, the generation of ice in spherical mesopore occurred at nearly homogeneous nucleation temperature (HNT) of bulk aqueous solution. As increasing concentration, the generation of ice in spherical mesopore disappeared. In the high concentration, the solution confined in spherical mesopore and micropore simultaneously froze at 190 K. This freeze temperature of solution in spherical mesopore was lower than HNT of bulk aqueous solution. Therefore, aqueous solution confined with mesopore may undergo rather vitrification than crystallization. Dynamics of water far and near sodium cation were studied by ^2H NMR T_1 and ^{23}Na NMR T_1 . Rotational correlation time of water in SBA-16 exhibited some variability. The correlation time of reconfiguration of water near sodium cation was nearly single. The width of distribution of correlation time decreased with increasing concentration. The correlation time of the isotropic rotation of water in the pores of SBA-16 followed Arrhenius behaviour above 190 K. Activation energy of water near sodium cation was lower than that far sodium cation.

Chapter 6 Hydration water of proteins crystal

Solid state ^2H NMR was used to investigate changes in the structure and dynamics of hydration waters of bovine serum albumin (BSA) due to glass transitions. The ^2H NMR spectra were separated into fast and slow components based on differences in spin-lattice relaxation time T_1 . The fast components corresponded to water molecules interacting with protein while the slow components were the water molecules similar to bulk water and deuterons of the protein backbone. Simulation analysis of the ^2H NMR spectra of the fast components was used to assess the mode and rate of motions of hydration waters around the protein. At low temperatures, the water molecules underwent a 180° flip and slow reorientation in the tetrahedral sites. The distribution of the rate of the 180° flip and the D-O-D angle of water molecules were clarified. The distribution of the D-O-D angle of water molecules spread with decreasing temperature. The marked slowing down in the reorientation of water molecules was observed at a glass transition of around 200 K, which is linked to the disordered region of the protein. In contrast, the 180° flip of water molecules occurred frequently, even below 200 K. A freeze of the 180° flip of water molecules was observed around the glass transition temperature of 110 K, where primary hydrate water formed a direct hydrogen bond with the protein, making it perfectly immobile.

1. ^2H NMR spectrum and T_1

Figure 6-1 shows the temperature dependence of the ^2H NMR broad-line spectrum. Above 273 K, a sharp spectrum due to the rapid isotropic rotation of water molecules was mainly observed. Below 273 K, a broad component with peaks at about ± 60 kHz due to the freezing of the motions of hydration waters appeared in the spectrum and its intensity increased with decreasing temperature. The line width of the central component increased with decreasing temperature. The broad central component below 213 K indicates the existence of the 180° flip of water molecules representing the distribution of the D-O-D angle. The central component of the spectrum disappeared and the ^2H NMR spectrum became an almost rigid powder pattern below $T_g = 110$ K accompanied by the freezing of primary hydrate water.

Figure 6-2 shows partially relaxed ^2H NMR spectra for the inversion recovery method at 203 K. As shown in the spectrum at a recovery time of $t_r = 10$ ms, recovery of the central sharp component was faster than that of the broad component. Figure 6-3 shows the recovery of magnetization for the inversion recovery method. The recovery of magnetization was analyzed by two-component fitting using Equation 6-1.

$$M(t_r)/M_0 = A_f \exp\left(- (t_r / T_{1f})^{\beta_f}\right) + (1 - A_f) \exp\left(- (t_r / T_{1s})^{\beta_s}\right) \quad \text{Equation 6-1}$$

Here, $M(t_r)$ is the magnetization at recovery time t_r and M_0 is the thermal-equilibrium value of magnetization. A_f is the ratio of the fast component. T_{1f} , β_f and T_{1s} , β_s are the spin-lattice relaxation times and the stretching parameters for fast and slow components, respectively. α shows imperfection in the 180° pulse. The deuterated parts in the protein backbone as well as water molecules undergoing slow motion are considered to be included in the slow component. Only one component was observed below 160 K. The mean T_{1f} and T_{1s} values were obtained by Ref. [102, 103, 104].

$$\langle T_{1i} \rangle = \frac{T_{1i}}{\beta_i} \Gamma\left(\frac{1}{\beta_i}\right), \quad (i = f, s) \quad \text{Equation 6-2}$$

where $\Gamma(x)$ is the Gamma function.

Figure 6-4 shows the temperature dependence of $\langle T_1 \rangle$ for fast and slow components. $\langle T_{1s} \rangle$ increased with decreasing temperature. The minimum of $\langle T_{1f} \rangle$ was observed around 230 K. $\langle T_{1f} \rangle$ is predicted to be dominated by the isotropic rotation of water molecules. For the isotropic rotation of water molecules, ^2H NMR T_1 is written as Equation 3-12. The minimum value of T_1 was estimated to be 1.5×10^{-3} s from Equation 3-12 and Equation 3-13 using the quadrupole interaction parameters of $e^2qQ/h = 230$ kHz and $\eta = 0$ which were obtained from the line shape of the ^2H NMR spectrum at low temperatures. The observed $\langle T_{1f} \rangle$ minimum (5×10^{-3} s) was longer than this calculated value. This result suggests the distribution of the correlation time τ . When a distribution of correlation time exists, $J(\omega)$ is well described by the Cole-Cole spectral density (Equation 3-18) [108] where τ_{cc} and α_{cc} are the correlation time at the maximum position and the width of distribution, respectively. From the minimum of $\langle T_{1f} \rangle$, $\alpha_{cc} = 0.52$ was estimated. Using this α_{cc} value and Equation 3-12 and Equation 3-18, τ_{cc} was estimated from $\langle T_{1f} \rangle$.

Figure 6-5 shows the temperature dependence of τ_{cc} . An Arrhenius type temperature dependence was observed for τ_{cc} . The change in the slope of $\log(\tau_{cc})$ vs. the $1/T$ plot was observed around 200 K. The activation energy of the motion of water molecules was obtained as 57 and 35 kJmol⁻¹ above and below 200 K, respectively. The glass transition around 200 K was caused by the rearrangement motion of the disordered region in the protein [62, 63]. Therefore, the dynamics of hydration waters is affected by freezing of the disordered region in the protein accompanied with a glass transition. The decrease in activation energy at low temperatures indicates a change of the motional mode of hydration water at around 200 K.

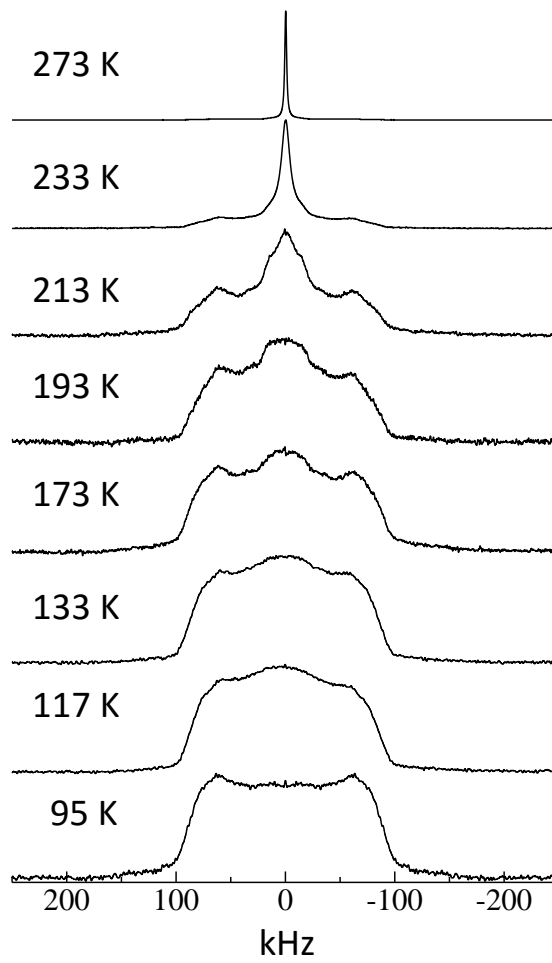


Figure 6-1 Temperature dependence of ^2H NMR spectrum for BSA.

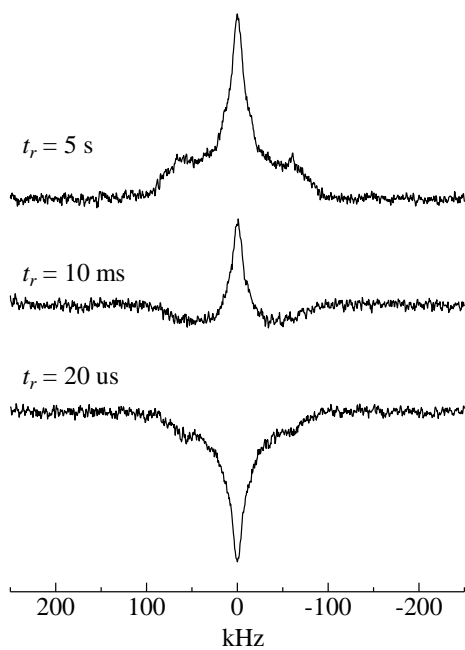


Figure 6-2 Partially relaxed ^2H NMR spectrum of BSA for inversion recovery method at 233 K. t_r shows the recovery time after a 180° pulse.

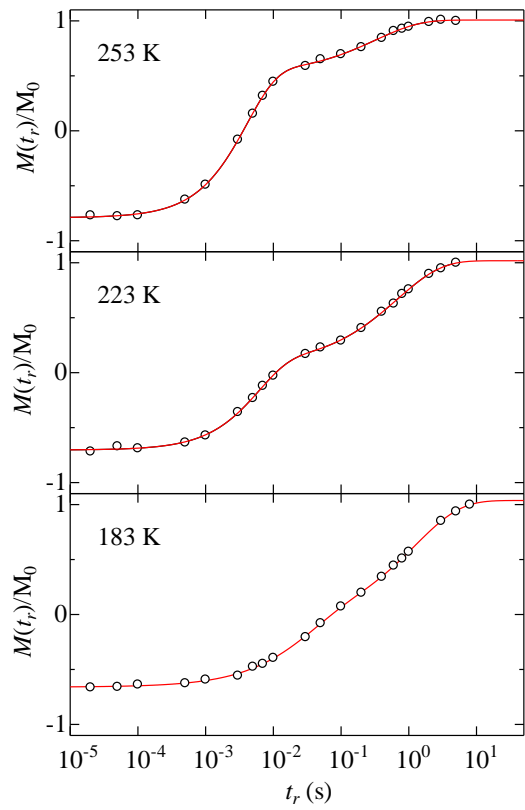


Figure 6-3 Magnetization recovery for the inversion recovery method. (a) 253 K, (b) 223 K, (c) 183 K. Solid lines show theoretical fitting of two stretched exponential functions of Equation 6-1 in the text.

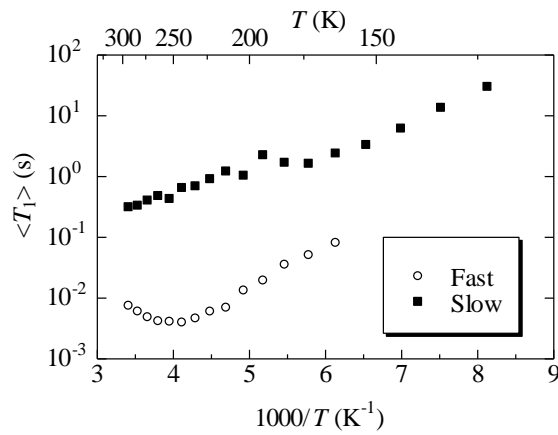


Figure 6-4 Temperature dependence of ^2H NMR mean spin-lattice relaxation time $\langle T_1 \rangle$ for BSA. Solid and open circles show for the fast component ($\langle T_{1f} \rangle$) and the slow component ($\langle T_{1s} \rangle$), respectively.

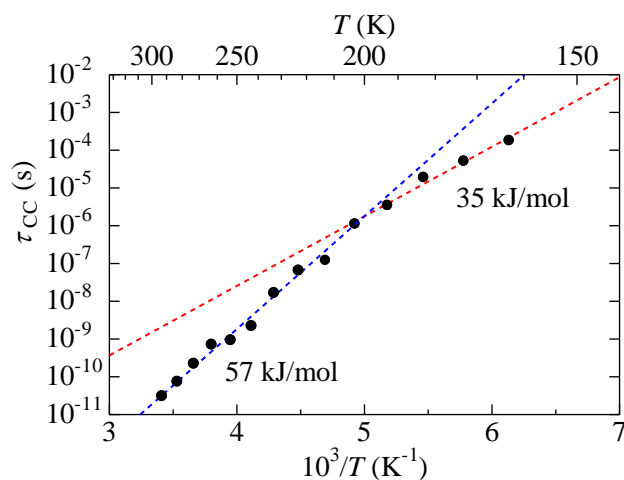


Figure 6-5 Temperature dependence of correlation time τ_{cc} obtained from ^2H NMR for the fast component.

2. ^2H NMR partially relaxed spectrum

In order to obtain the ^2H NMR spectrum of the fast component, the partially relaxed spectra for saturation recovery were measured. The spectrum of the fast component was selectively obtained by setting recovery time t_r after saturation pulses as $1/10$ of the $\langle T_1 \rangle$ value of the slow component. Figure 6-6 shows the ^2H NMR spectrum of the fast component. The ^2H NMR spectrum of the fast component observed at 233 K showed a sharp peak due to isotropic rotation or a jump among the tetrahedral sites of the water molecule. The intensity of the broad component with a line width of ca. ± 60 kHz increased with decreasing temperature. Moreover, the line width of the central portion of the spectrum broadened with decreasing temperature. Analysis of the ^2H NMR spectrum of the fast component was performed using spectral simulation [100]. The motions and angles of water molecules used for the simulation analysis are shown in Figure 6-7. The combination of a 180° flip and slow jump to the other two sites in the tetrahedral sites (i.e., reorientation of water molecules) was considered in the motions of water molecules. k_{180° and k_{re} are the rates of the 180° flip and the slow jump to the other two sites in the tetrahedral sites of water molecules, respectively in Figure 6-7. θ is the angle between the electric field gradients in two deuterons of a water molecule and almost corresponds to the D-O-D angle except for intermolecular interactions. The distributions of k_{180° , k_{re} and θ were considered for the simulation of the ^2H NMR spectrum. The intensity of the partially relaxed spectrum depends on T_1 which is dominated by jumping rate k_{180° . The

reduction factor $g_{red}(k_{180^\circ})$ for the signal intensity due to partial relaxation is written as

$$g_{red}(k_{180^\circ}) = 1 - \exp\left(-\frac{t_r}{T_1}\right) \quad \text{Equation 6-3}$$

T_1 for the 180° flip of water molecules was obtained by Equation 3-14 where τ and k_{180° are related as $k_{180^\circ} = (2\tau)^{-1}$. Each spectral component was multiplied by $g_{red}(k_{180^\circ})$ in the simulation of the partially relaxed ^2H NMR spectrum. The distribution of k_{180° was estimated using the distribution of correlation time τ obtained from $\langle T_{1f} \rangle$. For the distribution of k_{re} , Cole-Cole distribution (Equation 3-17) with same distribution width parameter α_{cc} as k_{180° and containing only mean value of k_{re} as parameter was used. The Gaussian function was assumed for the distribution of θ . The distribution centers of k_{re} and θ and the distribution width of θ were determined from spectral fitting (Figure 6-6). Figure 6-8 shows the distribution of k_{re} , k_{180° and θ . The center of k_{re} was lower than that of k_{180° by about double digits. The effect of reorientation of water molecules on the spectrum was not observed in the spectrum at 173 K. On the contrary, a large amount of water molecules underwent a 180° flip with more than 10^4 Hz even at 173 K. Thus, the behavior of water molecules observed in the ^2H NMR spectra of the fast component was largely different from that of bulk waters [101]. The high mobility of unfreezeable water, which constructs a shell layer, and bound water, which attaches directly on the protein surface even at low temperatures, has been shown for BSA from dielectric measurements [74]. Therefore, the water molecules observed in the ^2H NMR spectra of the fast component are considered to be near to the protein and interacting with it. Although the motions of water molecules near protein are restricted and the reorientation of water molecules is suppressed by freezing of the disordered region in the protein due to a glass transition around 200 K, those water molecules undergo a 180° flip even below 200 K. The rate of the 180° flip of the water molecules near protein decreases with decreasing temperature. The rigid pattern of the ^2H NMR spectrum below 110 K (Figure 6-1) indicates freezing of the 180° flip of those water molecules. The decrease in the activation energy obtained from the temperature dependence of τ_{cc} below 200 K corresponds to the change from the tetrahedral jump to the 180° flip of the water molecules. The distribution width of the D-O-D angle (θ) increased with decreasing temperature, as shown in Figure 6-8. In fact, θ is the angle between the electric field gradients in two deuterons of a water molecule. Therefore, intermolecular interactions related to the hydrogen bond affect θ . The increase in the distribution of θ shows an increase in the interactions between water molecules and protein accompanied by a slowing down of motions of the water molecules.

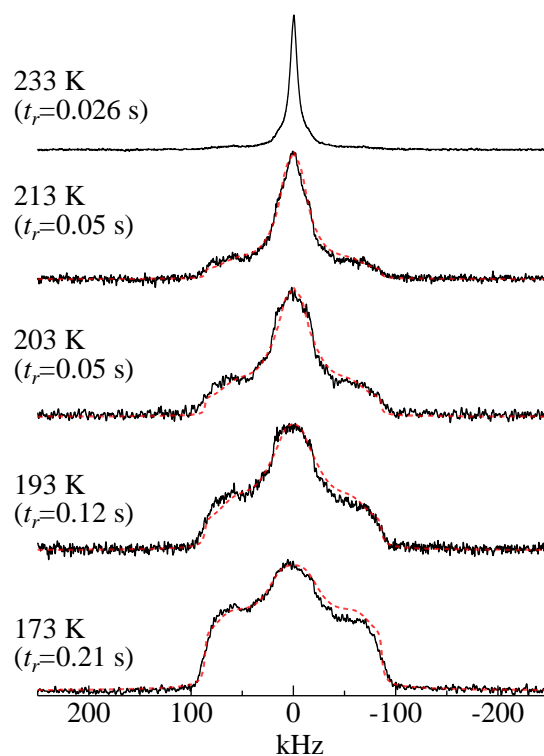


Figure 6-6 ^2H NMR spectra of the fast component for BSA. t_r shows the recovery time after saturation pulses. Solid lines are observed spectra. Broken lines are simulated spectra assuming motions of water molecules in Figure 6-7

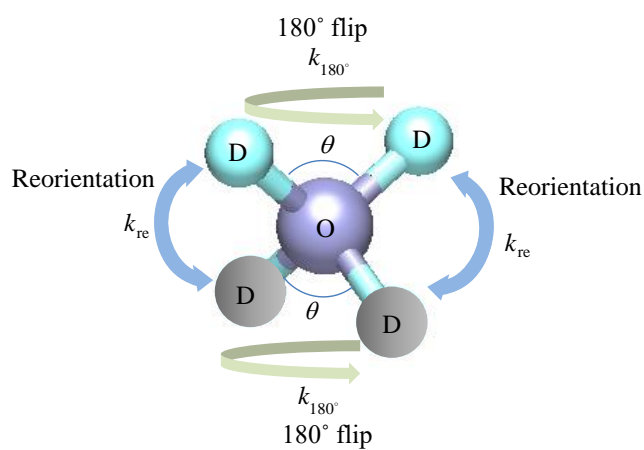


Figure 6-7 Motion of water molecules used for simulation of the ^2H NMR spectrum. ^2H NMR spectrum around 200 K could be well reproduced by a combination of the 180° flip and a slow jump to the other two sites in the tetrahedral sites (reorientation of water molecules).

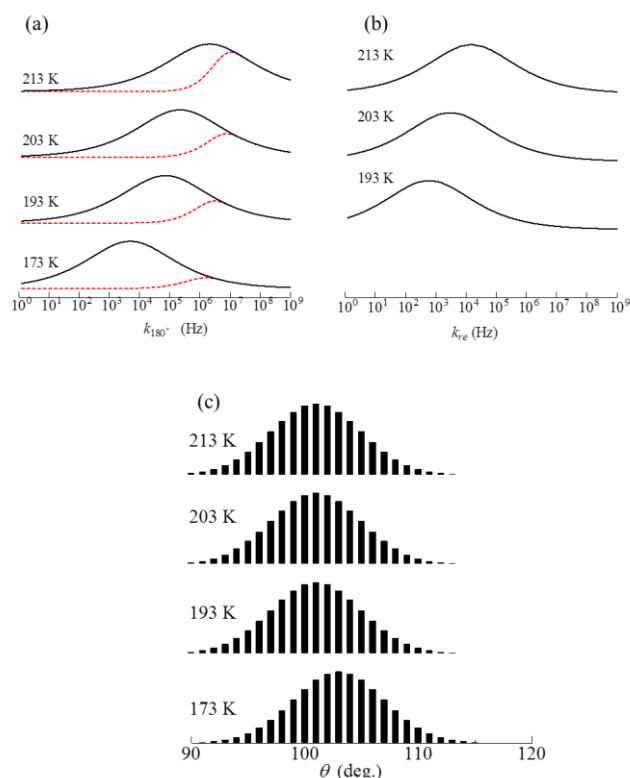


Figure 6-8 Distribution of rates of the 180° flip (a), rates of reorientation k_{re} (b) and angles θ (c) for water molecules. Red broken lines in (a) show distribution of the signal component affected by partial relaxation.

3. Conclusion

In this chapter, we clarified the motions and structures of the hydrate waters around low-temperature glass transitions. The isotropic rotation of water molecules near protein are restricted by freezing of the disordered region in the protein around the glass transition temperature ($T_g = 200$ K) and the 180° flip becomes a dominant motion for water molecules below T_g . The gradual slowing down of the 180° flip of water molecules near protein was observed in the temperature range of 200-110 K. The distribution width of the D-O-D angle of water molecules increased gradually by decreasing the rates of motions of water molecules at low temperatures. Freezing of the 180° flip of water molecules near the protein was observed around another glass transition temperature ($T_g = 110$ K).

Chapter 7 Conclusion

Thermal and dynamic property of water confined with three kinds of nanoscale spaces was investigated by solid-state NMR and DSC. They are water confined with mesoporous silica SBA-16, water in sodium chloride aqueous solution confined with SBA-16, and hydration water in the proteins (bovine serum albumin, BSA) crystal, respectively.

Firstly, water confined with SBA-16 was maintained. Rotational correlation time of water confined with spherical mesopores of SBA-16 followed Vogel-Fulcher-Tammann relation, which reflects the formation and growth of clusters of fragile water for changing to strong water. Water in micropores of SBA-16 frozen at nearly 200 K. Above 200 K, activation energy of water in micropores exhibited anomaly large values (63-114 kJ/mol), which was interpreted as non-Arrhenius behavior.

Secondly, water in sodium chloride aqueous solution confined with SBA-16 was maintained. Rotational correlation time of water confined with SBA-16 followed Arrhenius relation. Water in spherical mesopores and micropores simultaneously froze at nearly 190 K in the high concentration region. This freeze temperature of solution in spherical mesopore was lower than HNT of bulk aqueous solution. Therefore, aqueous solution confined with mesopore may undergo rather vitrification than crystallization.

Lastly, water in protein crystal was maintained. 180° flip and reorientation of water was observed between 220 K and 190 K. Freezing of the 180° flip of water molecules near the protein was observed around glass transition temperature ($T_g = 110$ K).

As a whole, rotational correlation time of water confined with these nanoscale spaces has a wide distribution in common. Isotropic rotation or reorientation of water with these nanoscale spaces trend to freeze at nearly 190 K.

Reference

- [1] T. Yanagisawa, T. Shimizu, K. Kuroda and C. Kato, *Bull. Chem. Soc. Jpn.*, vol. 63, p. 988, 1990.
- [2] C. T. Kresge, M. E. Leonowicz, W. J. Roth, J. C. Vartuli and J. C. Vartuli, *Nature*, vol. 359, p. 710, 1992.
- [3] D. Y. Zhao, J. L. Feng, Q. S. Huo, N. Melosh, G. H. Fredrickson, B. F. Chmelka and G. D. Stucky, *Science*, vol. 279, p. 548, 1998.
- [4] K. Morishige and K. Kawano, *J. Chem. Phys.*, vol. 110, p. 4867, 1999.
- [5] S. Takahara, M. Nakano, S. Kittaka, Y. Kuroda, T. Mori, H. Hamano and T. Yamaguchi, *J. Phys. Chem.*, vol. 103, p. 5814, 1999.
- [6] A. Schreiber, I. Ketelsen and G. H. Findenegg, *Phys. Chem. Chem. Phys.*, vol. 3, p. 1185, 2001.
- [7] A. Faraone, L. Liu, C.-Y. Mou, C.-W. Yen and S.-H. Chen, *J. Chem. Phys.*, vol. 121, p. 10843, 2004.
- [8] C. Alba-Simionesco, B. Coasne, G. Dosseh, G. Dudziak, K. E. Gubbins, R. Radhakrishnan and M. Sliwinska-Bartkowiak, *J. Phys. Condens. Matter*, vol. 18, p. R15, 2006.
- [9] S. Kittaka, S. Ishimaru, M. Kuranishi, T. Matsuda and T. Yamaguchi, *Phys. Chem. Chem. Phys.*, vol. 8, p. 3223, 2006.
- [10] C. Marcolli, *Atmos. Chem. Phys.*, vol. 14, p. 2071, 2014.
- [11] K. Yoshida, T. Yamaguchi, S. Kittaka, M.-C. Bellissent-Funel and P. Fouquet, *J. Chem. Phys.*, vol. 129, p. 054702, 2008.
- [12] M. Oguni, Y. Kanke, A. Nagoe and S. Namba, *J. Phys. Chem. B*, vol. 115, p. 14023, 2011.
- [13] S. Kittaka, Y. Ueda, F. Fujisaki, T. Iiyama and T. Yamaguchi, *Phys. Chem. Chem. Phys.*, vol. 13, p. 17222, 2011.
- [14] M. Erko, D. Wallacher, A. Hoell, T. Hauss, I. Zizak and O. Paris, *Phys. Chem. Chem. Phys.*, vol. 14, p. 3852, 2012.
- [15] S. Kittaka, T. Urabe and I. Tominaga, *Ads. Sci. Tech.*, vol. 33, p. 749, 2015.
- [16] S. Kittaka, S. Takahara, H. Matsumoto, Y. Wada, T. J. Satoh and T. Yamaguchi, *J. Chem. Phys.*, vol. 138, p. 204714, 2013.
- [17] A. K. Soper, *Nature Mater.*, vol. 13, p. 671, 2014.
- [18] R. Mancinelli, F. Bruni and M. A. Ricci, *J. Phys. Chem. Lett.*, vol. 1, p. 1277, 2010.
- [19] R. Mancinelli, F. Bruni and M.A. Ricci, *J. Mol. Liq.*, vol. 159, p. 42, 2011.

- [20] L Liu, A Faraone, C.-Y. Mou, C.-W. Yen and S.-H. Chen, *J. Phys. Condens. Matter*, vol. 16, p. S5403, 2004.
- [21] L. Liu, S.-H. Chen, A. Faraone., C.-W. Yen, C.-Y. Mou, A. I Kolesnikov, E. Mamontov and J. Leao, *J. Phys. Condens. Matter*, vol. 18, p. S2261, 2006.
- [22] B. Grunberg, T. Emmler, E. Gedat, I. Shenderovich, G. H. Findenegg, H.-H. Limbach and G. Buntkowsky, *Chem. Eur. J.*, vol. 10, p. 5689, 2004.
- [23] F. Mallamace, M. Broccio, C. Corsaro, A. Faraone, U. Wanderlingh, L. Liu, C.-Y. Mou and S.-H. Chen, *Chem. Phys.*, vol. 124, p. 161102, 2006.
- [24] F. Mallamace, M. Broccio, C. Corsaro, A. Faraone, L. Liu, C.-Y. Mou and S.-H. Chen, *J. Phys. Condens. Matter*, vol. 18, p. S2285, 2006.
- [25] J. B. W Webber, J. C. Dore, J. H. Strange, R. Anderson and B. Tohidi, *J. Phys. Condens. Matter*, vol. 19, p. 415117, 2007.
- [26] E. Tombari, G. Salvetti and G. P. Johari, *J. Phys. Chem. C*, vol. 116, p. 2702, 2012.
- [27] S. Kittaka, K. Sou, T. Yamaguchi and K. Tozaki, *Phys. Chem. Chem. Phys.*, vol. 11, p. 8538, 2009.
- [28] F. Mallamace, M. Broccio, C. Corsaro, A. Faraone, D. Majolino, V. Venuti, L. Liu, C.-Y. Mou and S.-H. Chen, *Proc Natl Acad Sci U S A.*, vol. 104(2), p. 424, 2007 Jan 9.
- [29] C. E. Bertrand, Y. Zhang and S.-H. Chen, *Phys. Chem. Chem. Phys.*, vol. 15, p. 721, 2013.
- [30] D. Y. Zhao, Q. S. Huo, J. L. Feng, B. F. Chmelka and G. D. Stucky, *J. Amer. Chem. Soc.*, vol. 120, p. 548, 1998.
- [31] Y. Sakamoto, M. Kaneda, O. Terasaki, D. Y. Zhao, J. M. Kim and G. D. Stucky, H. J. Shin and R. Ryoo, *Nature*, vol. 408, p. 449, 2000.
- [32] K. Morishige, H. Yasunaga, R. Denoyel and V. Wernert, *J. Phys. Chem. C*, vol. 111, p. 9488, 2007.
- [33] K. Morishige and K. Yoshida, *J. Phys. Chem. C*, vol. 114, p. 7095, 2010.
- [34] N. H. Fletcher, *The Chemical Physics of Ice*(Japanese edition), Cambridge University Press(Kyoritsu Shuppan), 1970(1974), p. 74.
- [35] H. Yang, J. Li, J. Yang, Z. Liu, Q. Yang and C. Li, *Chem. Commun.*, p. 1086, 2007.
- [36] L.-F. Gutierrez, S. Hamoudi and K. Belkacemi, *Catalysts*, vol. 1, p. 97, 2011.
- [37] R. Maheswari, M. P. Pachamuthu, A. Ramanathan and B. Subramaniam, *Ind. Eng. Chem. Res.*, vol. 53, p. 18833, 2014.
- [38] S. M. Sarkar, M. E. Ali, M. L. Rahman and M. M. Yusoff, *J. Nanomater.*, vol. 2014, pp. Article ID 123680, 5 pages, 2014.

- [39] R. Maheswari, V. V. Srinivasan, A. Ramanathan, M. P. Pachamuthu, R. Rajalakshmi and G. Imran, *J. Porous Mat.*, vol. 22, p. 705, 2015.
- [40] S. M. Sarkar, M. L. Rahman and M. M. Yusoff, *New J. Chem.*, vol. 39, p. 3564, 2015.
- [41] P.-G. Choi, T. Ohno, N. Fukuhara, T. Masui and N. Imanaka, *J. Adv. Ceram.*, vol. 4, p. 71, 2015.
- [42] R. Rockmann and G. Kalies, *J Colloid Interface Sci.*, vol. 315, p. 1, 2007.
- [43] D. Zhao, Q. Huo, J. Feng, B. F. Chmelka and G. D. Stucky, *J. Am. Chem. Soc.*, vol. 120, p. 6024, 1998.
- [44] Y. Sakamoto, M. Kaneda, O. Terasaki, D. Y. Zhao, J. M. Kim, G. Stucky, H. J. Shin and R. Ryoo, *Nature*, vol. 408, p. 449, 2000.
- [45] T. -W. Kim, R. Ryoo, M. Kruk, K. P. Gierszal, M. Jaroniec, S. Kamiya and O. Terasaki, *J. Phys. Chem. B*, vol. 108, p. 11480, 2004.
- [46] P. Van Der Voort, M. Benjelloun and E. F. Vansant, *J. Phys. Chem. B*, vol. 106, p. 9027, 2002.
- [47] O. C. Gobin, Y. Wan, D. Zhao, F. Kleitz and S. Kaliaguine, *J. Phys. Chem. C*, vol. 111, p. 3053, 2007.
- [48] E. M. Rivera-Muñoz and R. Huirache-Acuña, *Int. J. Mol. Sci.*, vol. 11, p. 3069, 2010.
- [49] O. C. Gobin, Q. Huang, H. Vinh-Thang, F. Kleitz, M. Eić and S. Kaliaguine, *J. Phys. Chem. C*, vol. 111, p. 3059, 2007.
- [50] O. Petrov and I. Furo, *Phys. Chem. Chem. Phys.*, vol. 13, p. 16358, 2011.
- [51] S. Xu, G. C. Simmons, T. S. Mahadevan, G. W. Scherer, S. H. Garofalini and C. Pacheco, *Langmuir*, vol. 25, p. 5084, 2009.
- [52] M. C. F. Wander and K. L. Shuford, *J. Phys. Chem. C*, vol. 114, p. 20539, 2010.
- [53] R. K. Kalluri, D. Konatham and A. Striolo, *J. Phys. Chem. C*, vol. 115, p. 13786, 2011.
- [54] T. A. Ho, D. Argyris, D. R. Cole and A. Striolo, *Langmuir*, vol. 28, p. 1256, 2012.
- [55] I. Kalcher and J. Dzubiella, *Phys. Rev. E*, vol. 88, p. 062312, 2013.
- [56] L. Zhao, L. Pan, Z. Cao and Q. Wang, *Chem. Phys. Lett.*, vol. 647, p. 170, 2016.
- [57] T. M. Eggenhuisen, M. J. van Steenberg, H. Talsma, P. E. de Jongh and K. O. de Jong, *J. Phys. Chem. C*, vol. 113, p. 16785, 2009.
- [58] E. Mamontov, D. R. Cole, S. Dai, M. D. Pawel, C. D. Liang, T. Jenkins, G. Gasparovic and E. Kintzel, *Chem. Phys.*, vol. 352, p. 117, 2008.
- [59] K. Watanabe and M. Mizoguchi, *Cold Reg. Sci. Technol.*, vol. 34, p. 103, 2002.
- [60] J. Hwang and H. Daiguji, *Langmuir*, vol. 29, p. 2406, 2013.
- [61] K. Miyata, H. Kanno, T. Niino and K. Tomizawa, *Chem. Phys. Lett.*, vol. 354, p. 51, 2002.

- [62] W. Doster, S. Cusack and W. Petry, *Nature*, vol. 337, p. 754, 1989.
- [63] B. F. Rasmussen, A. M. Stock, D. Ringe and G. A. Petsko, *Nature*, vol. 357, p. 423, 1992.
- [64] A. L. Lee and A. J. Wand, *Nature*, vol. 411, p. 501, 2001.
- [65] J. H. Roh, V. N. Novikov, R. B. Gregory, J. E. Curtis, Z. Chowdhuri and A. P. Sokolov, *Phys. Rev. Lett.*, vol. 95, pp. 038101-1, 2005.
- [66] K. Kawai, T. Suzuki and M. Oguni, *Thermochim. Acta*, vol. 431, p. 4, 2005.
- [67] K. Kawai, T. Suzuki and M. Oguni, *Biophys. J.*, vol. 90, p. 3732, 2006.
- [68] Y. Miyazaki, T. Matsuo and H. Suga, *J. Phys. Chem. B*, vol. 104, p. 8044, 2000.
- [69] C. Bon, A. J. Dianoux, M. Ferrand and M. S. Lehmann, *Biophys. J.*, vol. 83, p. 1578, 2002.
- [70] J. H. Roh, J. E. Curtis, S. Azzam, V. N. Novikov, I. Peral, Z. Chowdhuri, R. B. Gregory and A. P. Sokolov, *Biophys. J.*, vol. 91, p. 2573, 2006.
- [71] S. -H. Chen, L. Liu, E. Fratini, P. Baglioni, A. Faraone and E. Mamontov, *Proc. Natl. Acad. Sci. U. S. A.*, vol. 103, p. 9012, 2006.
- [72] P. Kumar, Z. Yan, L. Xu, M. G. Mazza, S. V. Buldyrev, S. -H. Chen, S. Sastry and H. E. Stanley, *Phys. Rev. Lett.*, vol. 97, pp. 177802-1, 2006.
- [73] G. Sartor, A. Hallbrucker and E. Mayer, *Biophys. J.*, vol. 69, p. 2679, 1995.
- [74] N. Miura, Y. Hayashi, N. Shinyashiki and S. Mashimo, *Biopolymers*, vol. 36, p. 9, 1995.
- [75] J. Eden, P. R. C. Gascoyne and R. Pethig, *J. Chem. Soc. Faraday Trans. 1*, vol. 76, p. 426, 1980.
- [76] A. Yokoyama, H. Ishikawa, M. Shinohara, N. Shinyashiki, S. Yagihara and Y. Hayashi, *Proceedings of Flow Dynamics: the Second International Conference on Flow Dynamics, American Institute of Physics*, vol. CP832, p. 163, 2006.
- [77] N. Shinyashiki, W. Yamamoto, A. Yokoyama, T. Yoshinari, S. Yagihara, R. Kita, K. L. Ngai and S. Capaccioli, *J. Phys. Chem. B*, vol. 113, p. 14448, 2009.
- [78] J. E. Jentoft and R. G. Bryant, *J. Am. Chem. Soc.*, vol. 96, p. 297, 1974.
- [79] B. D. Hilton, E. Hsi and R. G. Bryant, *J. Am. Chem. Soc.*, vol. 99, p. 8483, 1977.
- [80] E. R. Andrew, D. J. Bryant and E. M. Cashell, *Chem. Phys. Lett.*, vol. 69, p. 551, 1980.
- [81] T. G. Pedersen, B. W. Sigurskjold, K. V. Andersen, M. Kjar, F. M. Poulsen, C. M. Dobson and C. Redfield, *J. Mol. Biol.*, vol. 218, p. 413, 1991.
- [82] G. Diakova, Y. A. Goddard, J. P. Korb and R. G. Bryant, *J. Magn. Reson.*, vol. 189, p. 166, 2007.
- [83] F. Mallamace, S. H. Chen, M. Broccio, C. Corsaro, V. Crupi, D. Majolino, V. Venuti, P.

- Baglioni, E. Fratini, C. Vannucci and H. E. Stanley, *J. Chem. Phys.*, vol. 127, pp. 045104-1, 2007.
- [84] P. Neudecker, P. Lundström and L. E. Kay, *Biophys. J.*, vol. 96, p. 2045, 2009.
- [85] B. Borah and R. G. Bryant, *Biophys. J.*, vol. 38, p. 47, 1982.
- [86] H. Peemoeller, F. G. Yeomans, D. W. Kydon and A. R. Sharp, *Biophys. J.*, vol. 49, p. 943, 1986.
- [87] L. T. Kakalis and T. F. Kumosinski, *Biophys. Chem.*, vol. 43, p. 39, 1992.
- [88] M. G. Usha, J. Speyer and R. J. Wittebort, *Chem. Phys.*, vol. 158, p. 487, 1991.
- [89] J. W. Mack, M. G. Usha, J. Long, R. G. Griffin and R. J. Wittebort, *Biopolymers*, vol. 53, p. 9, 2000.
- [90] Y. A. Goddard, J. -P. Korb and R. G. Bryant, *Biophys. J.*, vol. 91, p. 3841, 2006.
- [91] K. Schmidt-Rohr and H. W. Spiess, *Multidimensional Solid-state NMR and Polymers*, London: Academic Press, 1994.
- [92] R. R. Vold, "Deuterium NMR studies of dynamics in solids and liquid crystals," in *Nuclear Magnetic Resonance Probes of Molecular Dynamics*, Norwell, MA, Kluwer Academic Publishers, 1994, p. 27.
- [93] R. R. Vold and R. L. Vold, "Deuterium relaxation in molecular solids," in *Advances in Magnetic and Optical Resonance*, vol. 16, San Diego, Academic Press Inc, 1991, p. 85.
- [94] J. R. Long, R. Ebelhauser and R. G. Griffin, *J. Phys. Chem. A*, vol. 101, p. 988, 1997.
- [95] J. Kimura, T. Fukase, M. Mizuno and M. Suhara, *Z. Naturforsch.*, vol. 53a, p. 453, 1998.
- [96] M. Mizuno, Y. Hamada, T. Kitahara and M. Suhara, *J. Phys. Chem. A*, vol. 103, p. 4981, 1999.
- [97] M. Mizuno, T. Iijima and M. Suhara, *J. Phys. Condens. Matter*, vol. 12, p. 7261, 2000.
- [98] T. Iijima and M. Mizuno, *Chem. Phys. Lett.*, vol. 380, p. 736, 2003.
- [99] M. Mizuno, Y. Suzuki, K. Endo, M. Murakami, M. Tansho and T. Shimizu, *J. Phys. Chem. A*, vol. 111, p. 12954, 2007.
- [100] T. Araya, A. Niwa, M. Mizuno and K. Endo, *Chem. Phys.*, vol. 344, p. 291, 2008.
- [101] R. J. Wittebort, M. G. Usha, D. J. Ruben, D. E. Wemmer and A. Pines, *J. Am. Chem. Soc.*, vol. 110, p. 5668, 1988.
- [102] M. Vogel, *Phys. Rev. Lett.*, vol. 101, pp. 225701-1, 2008.
- [103] S. A. Lusceac, M. R. Vogel and C. R. Herbers, *Biochim. Biophys. Acta*, vol. 1804, p. 41, 2010.
- [104] S. A. Lusceac and M. Vogel, *J. Phys. Chem. B*, vol. 114, p. 10209, 2010.
- [105] M. Mehring, *Principles of High Resolution NMR in Solids*, Second, Revised and Enlarged Edition, Springer-Verlag Berlin Heidelberg New York, 1983.

- [106] K. E. Håland and B. Pedersen, *J. Chem. Phys.*, vol. 58, p. 3472, 1973.
- [107] D. E. Woessner, *Concepts in Magnetic Resonance*, vol. 13, p. 294, 2001.
- [108] P. A. Beckmann, *Phys. Rep.*, vol. 171, p. 85, 1988.
- [109] G. P. Johari, *J. Chem. Phys.*, vol. 130, p. 124518, 2009.
- [110] N. Bloembergen, E. M. Purcell and R. Pound, *Phys. Rev.*, vol. 73, p. 679, 1948.
- [111] M. Sattig and M. Vogel, *J. Phys. Chem. Lett.*, vol. 5, p. 174, 2014.
- [112] S. Kittaka, T. Miyatoh, M. Mizuno, K. Yoshida, T. Yamaguchi, M.-C. Bellissent Funel and P. Fouquet, *10th International Symposium on the Characterization of Porous Solids (COPS-X), Granada, 11-14 May, 2014*.
- [113] E. Whalley, *The Hydrogen Bond: Recent Theory and Experiments* vol 3, ed P Schuster, G Zundel and C Sandorfy (Amsterdam: North-Holland), 1976, p. chapter 29.
- [114] J. Sjostrom, J. Swenson, R. Bergman and S. Kittaka, *J. Chem. Phys.*, vol. 128, p. 154503, 2008.
- [115] T. Kim, R. Ryoo, M. Kruk, K. P. Gierszal, M. Jaroniec, S. Kamiya and O. Terasaki, *J. Phys. Chem. B*, vol. 108, p. 11480, 2004.
- [116] O. Mishima, *J. Chem. Phys.*, vol. 123, p. 154506, 2005.

Acknowledgment

Throughout the course of this study, I have received generous support from many people. Taking this opportunity, I would like to express my gratitude to the people.

My deepest appreciation goes to Professor Mizuno of Kanazawa University. Without his encouragement, this dissertation would not have materialized.

I received generous support containing sample preparation and DSC measurement from Professor Kittaka of Okayama University of Science. I am deeply grateful to him.

I have had the support and encouragement of Associate Professor Ida of Kanazawa University.

I have had the support and encouragement of Assistant Professor Ohashi of Kanazawa University.

Discussions with Dr. Kumagai and Dr. Umiyama have been illuminating. I want to thank them.

I want to thank all members of Kanazawa University Theoretical Chemistry Laboratory for their support in everyday life.

Finally, I thank my parents and my sisters for continuous support and encouragement.

Appendix

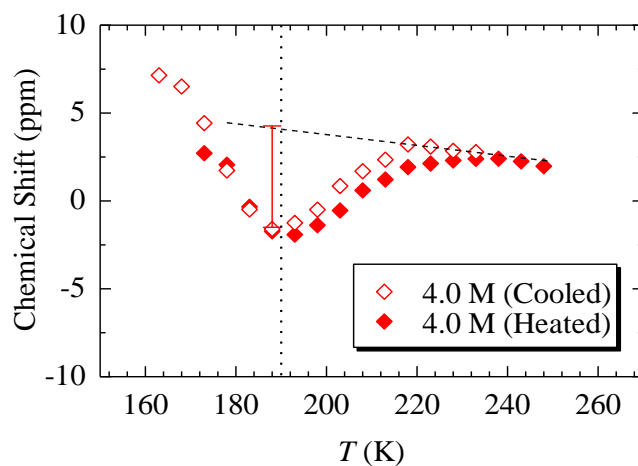


Figure A1 Temperature dependence of ^{23}Na NMR chemical shift for sodium chloride aqueous solution confined with SBA-16. The dotted line shows the freeze temperature of solution obtained by ^2H NMR.

The bar shows second order quadrupolar shift(δ_Q). $\delta_Q = 25000 \left(\frac{e^2qQ}{h} / \frac{\omega}{2\pi} \right)^2 \left(1 + \frac{\eta^2}{3} \right)$. The values

$\frac{e^2qQ}{h} = 1083$ kHz, $\eta = 0.77$ of $\text{NaCl} \cdot \text{D}_2\text{O}$ crystal [97] was used.